Aalto University
School of Electrical
Engineering

Jari-Matti Hannula

ON THE USE OF INTERMODULATION RESPONSE FOR CHARACTERIZING ANTENNAS

Thesis submitted in partial fulfillment of the requirements for the degree of Master of Science in Technology.
Espoo, May 20, 2015

Supervisor

Assistant Professor Ville Viikari

Advisor

M.Sc. (Tech.) Kimmo Rasilainen

Aalto University
School of Electrical
Engineering

Abstract

Author: Jari-Matti Hannula

Title: On the Use of Intermodulation Response for Characterizing Antennas

Date: May 20, 2015 **Number of pages:** 63

Unit: Department of Radio Science and Engineering

Field of research: Radio Science and Engineering

Supervisor: Assistant Professor Ville Viikari

Advisor: M.Sc. (Tech.) Kimmo Rasilainen

The intermodulation measurement technique enables the contactless measurement of transponder antennas by exploiting the inherent nonlinearity of the transponder to generate intermodulation products that can be measured. This intermodulation response can then be used to characterize the antenna.

In this master's thesis, this characterization technique is developed further. The theoretical intermodulation response for a harmonic transponder is derived, and this response is then used in measurements to characterize the transponder antenna. Limitations of the dynamic range of the measurement are discussed. The measurement can be performed using different arrangements of the measurement antennas. Three potential measurement geometries are discussed and compared: monostatic, bistatic, and multistatic. A measurement software is created for controlling the measurement.

The derived theory is validated by experiments. The measured intermodulation response of a harmonic transponder is compared with the theoretical response. The measurement technique is then used to measure the gain of the transponder antenna using bistatic geometry. The impedance matching of the transponder is also measured. The results show good agreement between the derived theory and the measurements. Based on the results, it can be said that the technique is well-suited for characterizing harmonic transponders.

Keywords: antenna measurements, harmonic radar, intermodulation distortion, radio frequency identification (RFID), transponders

Aalto-yliopisto
Sähkötekniikan korkeakoulu

Tiivistelmä

Tekijä:	Jari-Matti Hannula		
Työn nimi:	Intermodulaatiovasteen käyttö antennien karakterisoinnissa		
Päivämäärä:	20. toukokuuta 2015	**Sivumäärä:**	63
Yksikkö:	Radiotieteen ja -tekniikan laitos		
Tutkimusala:	Radiotiede ja -tekniikka		
Valvoja:	Apulaisprofessori Ville Viikari		
Ohjaaja:	DI Kimmo Rasilainen		

Intermodulaatiovasteeseen perustuva mittausmenetelmä mahdollistaa transponderiantennien langattoman mittaamisen hyödyntämällä transpondereille ominaista epälineaarisuutta. Epälineaarisuus tuottaa intermodulaatiotaajuuksia, jotka voidaan mitata. Mitattua vastetta voidaan käyttää antennin karakterisointiin.

Tässä diplomityössä kehitetään tätä karakterisointimentelmää. Työssä johdetaan teoreettinen intermodulaatiovaste harmoniselle transponderille, jota hyödynnetään mittauksissa transponderin antennin karakterisointiin. Mittausmenetelmän dynaamista aluetta rajoittavia tekijöitä tarkastellaan. Mittausta varten mittausantennit voidaan sijoittaa eri tavalla. Menetelmälle esitetään kolme mahdollista mittausgeometriaa: monostaattinen, bistaattinen ja multistaattinen. Eri geometrioita verrataan keskenään. Mittauksen ohjaamista varten kehitetään mittausohjelma.

Työssä esitetty teoria varmennetaan kokeellisesti. Harmonisen transponderin intermodulaatiovaste mitataan ja vastetta verrataan teoreettiseen vasteeseen. Mittausmenetelmää käytetään transponderin antennin vahvistuksen mittaamiseen hyödyntämällä bistaattista geometriaa. Myös transponderin impedanssisovitus mitataan. Mittaustulokset ja teoria vastaavat hyvin toisiaan. Mittausten perusteella menetelmä soveltuu hyvin harmonisten transponderien karakterisointiin.

Avainsanat: antennimittaukset, harmoninen tutka, intermodulaatiosärö, radiotaajuinen etätunnistus (RFID), transponderit

Preface

This thesis is based on research carried out at the Department of Radio Science and Engineering of Aalto University School of Electrical Engineering. I would like to take this opportunity to thank the people who have contributed to this thesis.

First of all, I would like to thank my supervisor Assistant Professor Ville Viikari for the opportunity to work on this topic. I am also grateful for his advice during the work.

My advisor M.Sc. (Tech.) Kimmo Rasilainen deserves my thanks for his guidance both in the practical aspects of radio engineering and also regarding writing. His insightful comments have always been a great help in improving my work.

Finally, I would like to thank my family and friends for their support throughout these years.

Espoo, May 20, 2015,

Jari-Matti Hannula

Contents

List of Abbreviations

AC	Alternating Current
AR	Axial Ratio
AUT	Antenna Under Test
BW	Bandwidth
DC	Direct Current
ESD	Electrostatic Discharge
GPIB	General Purpose Interface Bus
HF	High Frequency
IC	Integrated Circuit
IEEE	Institute of Electrical and Electronics Engineers
LF	Low Frequency
NFC	Near-Field Communication
PCB	Printed Circuit Board
RCS	Radar Cross Section
RF	Radio Frequency
RFID	Radio Frequency Identification
RX	Receiver
SAW	Surface Acoustic Wave
SINR	Signal-to-Interference-plus-Noise-Ratio
TX	Transmitter
UHF	Ultra High Frequency
USB	Universal Serial Bus
VNA	Vector Network Analyzer

List of Symbols

A	scaling parameter in gain measurements [1/W]
a	radius of a sphere [m]
C_{j0}	small-signal junction capacitance [F]
C_{p}	parasitic capacitance [F]
c	speed of light [m/s]
D	directivity of an antenna
D_{ant}	largest dimension of an antenna [m]
E_{IM}	intermodulation properties of the mixing element [1/W^2]
f	frequency [Hz]
f_0	fundamental frequency [Hz]
f_1	first fundamental frequency [Hz]
f_2	second fundamental frequency [Hz]
f_{IM}	frequency of intermodulation distortion [Hz]
f_{ref}	reference frequency [Hz]
G	gain
G_{R}	realized gain of an antenna
$G_{\mathrm{R,tag}}$	realized gain of a transponder antenna
G_{r}	gain of receiver antenna
G_{t}	transmitter gain
G_{ta}	gain of transmitter antenna
G_{tag}	gain of transponder antenna
$G_{\mathrm{tag,ref}}$	reference transponder gain
G_{tc}	gain of transmitter chain
I	current [A]
$I_{\mathrm{a,IM}}$	current through the antenna at the intermodulation frequency [A]
$I_{\mathrm{j,IM}}$	current through the diode junction at the intermodulation frequency [A]
IIP_3	input third-order intermodulation intercept point [W]
IP_3	third-order intermodulation intercept point [W]
$\jmath$	imaginary unit
k	Boltzmann constant

L	attenuation
L_{opt}	optimal attenuation
L_{s}	series inductance [H]
n	ideality factor
OIP_3	output third-order intermodulation intercept point [W]
P	power [W]
P_{adj}	adjusted transmitter input power [W]
P_{in}	input power [W]
P_{loss}	power dissipated due to losses [W]
P_{N}	noise power [W]
P_{NI}	total noise and interference power [W]
$P_{\mathrm{out,IM}}$	output power at the intermodulation frequency [W]
P_{rad}	radiated power [W]
P_{ref}	reference input power [W]
$P_{\mathrm{r,IM}}$	received intermodulation response [W]
$P_{\mathrm{r,max}}$	maximum received intermodulation response [W]
$P_{\mathrm{r,ss}}$	maximum valid small-signal response [W]
P_{t}	transmitter input power [W]
$P_{\mathrm{t,max}}$	maximum transmitter input power [W]
$P_{\mathrm{t,ss}}$	maximum transmitter input power for valid small-signal response [W]
q	elementary charge
R	resistance [Ω]
R_{A}	antenna resistance [Ω]
R_{D}	diode resistance [Ω]
R_{j}	small-signal junction resistance [Ω]
R_{L}	load resistance [Ω]
R_{loss}	loss resistance [Ω]
R_{rad}	radiation resistance [Ω]
R_{s}	series resistance [Ω]
r	distance [m]
r_{ff}	far-field distance [m]
r_{r}	distance from the receiver [m]
r_{t}	distance from the transmitter [m]
S	scattering parameter
S_{11}	reflection coefficient of the transponder
$S_{11,\mathrm{ref}}$	reflection coefficient at the reference frequency

S_{21}	coupling between the transmitter and the receiver
T	temperature [K]
t	time [s]
V_0	amplitude of the input voltage [V]
V_{DC}	direct current operating point of a nonlinear element [V]
V_{g}	voltage generated by an antenna [V]
v_{i}	input voltage [V]
v_{o}	output voltage [V]
X_{A}	antenna reactance [Ω]
X_{L}	load reactance [Ω]
Z_{A}	antenna impedance [Ω]
Z_{D}	diode impedance [Ω]
Z_{j}	junction impedance [Ω]
Z_{L}	load impedance [Ω]

γ	profile parameter
η_{m}	impedance mismatch factor
η_{rad}	radiation efficiency
θ	polar angle in spherical coordinates [°]
λ	wavelength [m]
ρ	reflection coefficient
Φ	junction potential [V]
ϕ	azimuthal angle in spherical coordinates [°]
Ω	transponder orientation angle
Ω_{R}	transponder orientation angle towards the receiver
Ω_{T}	transponder orientation angle towards the transmitter
Ω_{TR}	transponder orientation angle towards the transceiver
Ω_{Δ}	angular offset between the transmitter and the receiver
ω	angular frequency [rad/s]
ω_0	fundamental angular frequency [rad/s]
ω_1	first fundamental angular frequency [rad/s]
ω_2	second fundamental angular frequency [rad/s]

1. Introduction

A *transponder* (often called a *tag*) is a device that responds to the interrogation signal of a *reader* device by transmitting a modulated response. A transponder system generally consists of a reader and a transponder. There exist several kinds of transponders, but they are generally small devices, consisting of an antenna providing the wireless connection, and of an integrated circuit (IC) that provides the functionality.

A common transponder type is the *radio frequency identification* (RFID) transponder. The concept of RFID includes several different types of transponders, operating with different principles, at different frequencies, and with different read-out distances. The common factor is that the tag contains data that can be read or written wirelessly. The RFID market is growing rapidly, with applications in contactless smart cards, passports, animal identification, inventory management, access control, and many more [1].

There are also *harmonic transponders*. A harmonic transponder generates the response by multiplying the frequency of the incoming signal. Unlike RFID, a harmonic transponder has no memory. The response signal contains no information, other than whether the transponder is in the interrogation zone of the reader or not. The system is often referred to as *harmonic radar*, as its operation resembles that of radar. The concept for harmonic radar and transponders was first introduced in 1967 [2]. One of the first applications for the harmonic radar was its use as a vehicular radar [3], a system which was patented as well [4]. They are also used for locating avalanche victims buried under the snow [5]. The simple operation of harmonic transponders makes them easy to miniaturize, which has made them useful for tracking insects in biological and agricultural studies [6], [7].

In summer 2013, during my first year at the Department of Radio Science and Engineering of Aalto University, my task was to design a harmonic transponder. After some time, I finished a prototype design and then manufactured the transponder, illustrated in Fig. 1.1. The transponder consists of the designed antenna etched on a printed circuit board (PCB) substrate, a matching circuit (three inductors and two capacitors), and a diode.

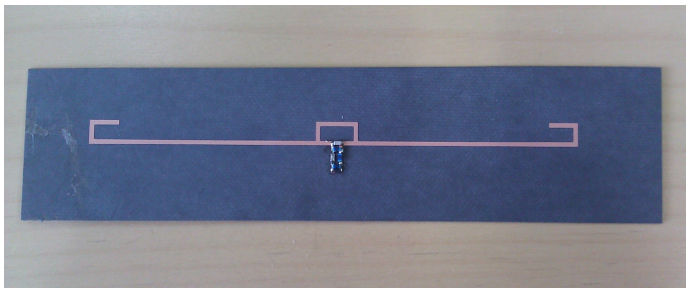

Fig. 1.1. A harmonic transponder designed by the author of this thesis in 2013.

The response of the transponder was then measured. However, it did not produce the expected response, with initial measurements failing to detect any response at all. With such a complex, five-component matching circuit, the most obvious reason for degraded performance was the difference between the simulated and manufactured matching network. The operation of the transponder is highly dependent on the impedance matching between the antenna and the diode at both the fundamental frequency and the second harmonic frequency.

Measuring the harmonic response of the transponder did not provide enough information regarding the operation of the antenna. The response suggested that the best matching did not occur at the design frequencies, but could not be used to investigate the actual location of the frequencies separately.

Antenna impedance is conventionally measured by connecting the antenna to a vector network analyzer (VNA). Transponder antennas are typically electrically small, and measuring such antennas is challenging. The measurement cables easily become a part of the radiating structure and thus alter the radiation. It might be necessary to equip the cable with a balun or an adapter, which further complicates the measurement. Additionally, the transponder impedance is often highly capacitive, far from the conventional 50-Ω level used by traditional measurement equipment. Obtaining reliable results is therefore difficult. Alternate measurement techniques could therefore be preferable, and especially techniques that do not involve a cable connection would be ideal.

For measuring the radiation properties of an RFID antenna, a dedicated reader can be used. Such measurement devices are commercially available, e.g., from Voyantic Ltd [8]. The measurement is based on finding the minimum power required for the tag to operate, and is mainly used for measuring the maximum read-out distance of the tag. Despite their apparent similarity, the fundamental operation of RFID differs from that of harmonic transponders. RFID measurements utilize the RFID principle to perform the measurements, and cannot therefore be used for characterizing harmonic transponders.

One well-researched wireless method is the radar cross section (RCS) technique. The technique is named like this because it depends on measuring the RCS of the antenna with different loads connected [9]. Changing the load changes the RCS of the antenna. By measuring the RCS with several loads (short, open, matched), the antenna properties can be solved. The method requires that the antenna can be measured when it is terminated with different loads, which is not practical for measuring a manufactured transponder.

Another measurement method initially developed for RFID is the intermodulation measurement technique, introduced in [10]. Instead of using the RFID principle, this technique exploits the nonlinear properties of the transponder chip to generate a response that is dependent on the antenna characteristics at one frequency. The diode used in a harmonic transponder is also a nonlinear element which generates intermodulation products. This method could therefore be potentially extended to apply to harmonic transponders as well.

The objective of this thesis is to develop a measurement system for taking advantage of the intermodulation measurement technique to investigate the suitability of the technique for characterizing harmonic transponders. This involves creating a software for controlling the measurement and collecting the measured data, after which another objective is to further develop the intermodulation measurement technique. Theoretical equations for the intermodulation response are derived, and the derived results are used to solve antenna characteristics of the measured transponders. The limitations and the dynamic range of the measurement method are examined. Different measurement geometries and their advantages are discussed. The theoretical results are then validated with experiments.

This thesis is structured as follows. Chapter 2 discusses common antenna parameters and general antenna measurement methods. In Chapter 3, the properties of nonlinear elements are examined. This includes effects such as distortion, rectification and mixing. The main novelty in this thesis is found in Chapter 4, in which the intermodulation measurement technique is analyzed. This includes deriving the equation for the theoretical intermodulation response, discussing the practical limitations of the model and the measurement, and potential measurement geometries for measuring the intermodulation response. The derived equations are experimentally verified, and the measurement procedures and results can be found in Chapter 5. Finally, Chapter 6 contains the summary and conclusions of the thesis.

2. Antenna characteristics and measurements

The antenna is an important component in all wireless systems. By definition, an antenna is the part of a transmitting or receiving system that is designed to radiate or to receive electromagnetic waves [11]. In other words, an antenna converts the guided waves of conductors or waveguides to unguided, radiating waves and vice versa. The operation and characteristics of an antenna are the same both in transmission and reception, i.e. antennas are reciprocal.

In the case of transponders, the antenna is responsible for the link between the transponder and the reader device. The operation of a transponder is highly dependent on the operation of the antenna. This can be described using several characteristics, the most common of which are explained in Section 2.1. The section focuses on parameters that can either be obtained using the intermodulation measurement technique or that must be considered when performing the measurement.

It is important to be able to measure these characteristics to verify the operation of the antenna. An antenna being measured is often referred to as *antenna under test* (AUT). This chapter describes some general antenna measurement methods. Conventional antenna measurements, which involve a cable connection to the AUT, are described. Additionally, due to the challenges involved in wired measurements of electrically small antennas, alternate measurement methods may be needed. The intermodulation measurement technique presented in this thesis is one such method. Other alternate measurement methods include the use of an RFID reader for RFID transponder measurements, and measurements based on antenna backscattering. These are described in Section 2.2 to give insight on other contactless measurement methods available. The intermodulation measurement technique is treated separately in Chapter 5.

2.1 Antenna characteristics

There are several parameters by which antennas can be characterized. These characteristics can be given as design parameters for an antenna, and different applications

prioritize different characteristics. This section explains the most common antenna characteristics.

2.1.1 Input impedance and impedance bandwidth

An antenna can be characterized using a circuit parameter *impedance*, which describes the ratio of the voltage and current at the antenna feed point. The impedance does not describe the radiation properties of the antenna, but it is important when considering the antenna as a part of the radio system. The operation of the system is highly dependent on the impedance matching between the antenna and the load connected to it, load referring to the system seen from the antenna input. If the antenna impedance is not properly matched to the load impedance, part of the received and transmitted power is reflected, resulting in mismatch loss. Depending on the severity of the mismatch, this can either degrade the performance of the system or completely negate the operation.

The *input inpedance* of an antenna (or simply *antenna impedance*) can be represented as

$$Z_\mathrm{A} = R_\mathrm{A} + \jmath X_\mathrm{A} = R_\mathrm{rad} + R_\mathrm{loss} + \jmath X_\mathrm{A}, \tag{2.1}$$

where R_A is the antenna resistance, which can be divided into radiation resistance R_rad and loss resistance R_loss, and X_A is the antenna reactance. $\jmath$ is the imaginary unit. The voltage generated (received) by the antenna can be represented as a voltage source V_g in series with the impedance. The connected system can be represented as a load impedance $Z_\mathrm{L} = R_\mathrm{L} + \jmath X_\mathrm{L}$, where R_L and X_L are the load resistance and reactance. Fig. 2.1 illustrates this equivalent circuit.

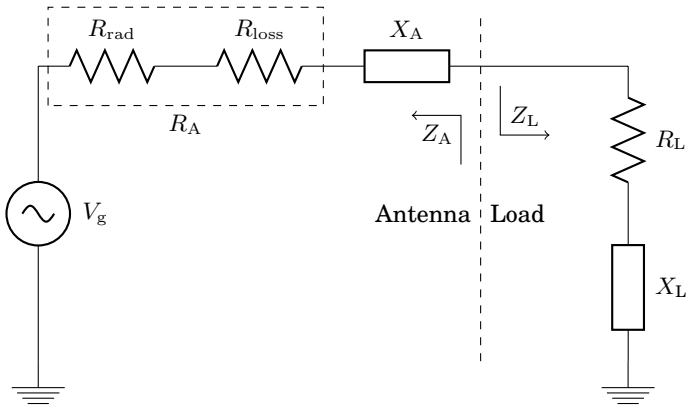

Fig. 2.1. The equivalent circuit of a receiving antenna connected to a load. For a transmitting antenna, the voltage source V_g would be located on the side of the load.

Depending on the antenna and load impedances, there may be some mismatch in the interface between the antenna and the load. This mismatch can be represented

using the *reflection coefficient*. The reflection coefficient between antenna and load impedances is

$$\rho = \frac{Z_\mathrm{L} - Z_\mathrm{A}^*}{Z_\mathrm{L} + Z_\mathrm{A}}, \tag{2.2}$$

where * indicates the complex conjugate.

Sometimes the reflection coefficient is denoted using the scattering parameter S_{11}, which describes the ratio of the returning and incoming waves. It should be noted that for a one-port system (such as a typical antenna), the reflection coefficient $\rho = S_{11}$. For a two-port system, the reflection coefficient ρ and S_{11} might not be equal, depending on the reflection properties of the second port.

The reflection coefficient describes the reflected voltage. For calculating reflected power, the *power reflection coefficient* can be used instead. The power reflection coefficient is defined as the square of the absolute value of the voltage reflection coefficient, $|\rho|^2$. The power reflection coefficient can be used to calculate the power accepted by the antenna. The accepted power is simply reduced by the amount of power reflected. One can define the *impedance mismatch factor*

$$\eta_\mathrm{m} = 1 - |\rho|^2 = \frac{4R_\mathrm{A}R_\mathrm{L}}{|Z_\mathrm{A} + Z_\mathrm{L}|^2}, \tag{2.3}$$

which describes the ratio of the accepted power and available power [12].

To minimize the reflection coefficient and to ensure minimal mismatch loss, the antenna and the load should be properly matched. From (2.2), the criteria for the antenna impedance can be derived to be

$$Z_\mathrm{A} = Z_\mathrm{L}^* \Rightarrow \begin{cases} R_\mathrm{A} = R_\mathrm{L} \\ X_\mathrm{A} = -X_\mathrm{L} \end{cases}. \tag{2.4}$$

When an antenna is matched according to (2.4), it is said to be conjugately matched. A conjugately matched antenna has $\rho = 0$ and $\eta_\mathrm{m} = 1$ (from (2.2) and (2.3)), so no power is lost due to reflections.

The antenna impedance is in practice frequency-dependent. The load impedance can be constant (typically $Z_\mathrm{L} = 50\ \Omega$) or it can change with frequency. Because of this, it is important to note that conjugate matching is possible at point frequencies only. Of course, in practice the reflection coefficient does not have to be exactly zero. Depending on the application, a reflection coefficient of, e.g., -6 or -10 dB can be adequate. By allowing a larger reflection coefficient, it is possible to increase the frequency range in which the antenna is well matched. The *impedance bandwidth* of an antenna can be defined as the bandwidth (BW) where the reflection coefficient is below some specified value, e.g., the aforementioned $|\rho| < -10$ dB.

2.1.2 Efficiency

Ideally, an antenna would radiate all the power fed to it. In practice, however, antennas are lossy. The *radiation efficiency* of an antenna is defined as the ratio of the total power radiated by an antenna and the net power accepted by the antenna from the connected transmitter [11], mathematically

$$\eta_{\text{rad}} = \frac{P_{\text{rad}}}{P_{\text{in}}} = \frac{P_{\text{rad}}}{P_{\text{rad}} + P_{\text{loss}}}, \tag{2.5}$$

where η_{rad} is the radiation efficiency, P_{rad} is the radiated power, and P_{in} is the accepted power. The accepted power can be represented as the sum of the radiated power P_{rad} and the dissipated power P_{loss}.

In (2.1), the total resistance of the antenna was separated into radiation and loss resistances. The power going to the radiation resistance is the power the antenna radiates. Similarly, the power in the loss resistance describes the power dissipated in the antenna. Using the relation between power and current, $P = \frac{1}{2}R|I|^2$, the efficiency can be represented using the resistances instead

$$\eta_{\text{rad}} = \frac{R_{\text{rad}}}{R_{\text{A}}} = \frac{R_{\text{rad}}}{R_{\text{rad}} + R_{\text{loss}}}. \tag{2.6}$$

The efficiency of an antenna can also be reported as *total efficiency*, which is defined as the ratio of radiated power and available power. The available power is the power supplied from the connected system. This definition therefore includes the losses due to reflections, so the total efficiency is

$$\eta_{\text{tot}} = \eta_{\text{m}}\, \eta_{\text{rad}} = (1 - |\rho|^2)\eta_{\text{rad}}. \tag{2.7}$$

2.1.3 Antenna size

An antenna occupies some physical volume. Usually the antenna size is constrained by the limits specified by the application, e.g., there is a specified space available for the antenna in a mobile phone. The constrained size can be problematic, as the antenna size should also be considered in relation to the wavelength at the frequency of operation. The size of an antenna relative to wavelength is known as the *electrical size* of the antenna. The physical size of the antenna does not necessarily correlate with the electrical size: a physically large antenna operating at low frequencies can be electrically small.

An electrically small antenna is defined as an antenna whose dimensions are such that it can be contained within a sphere whose diameter is small compared to a wavelength at the frequency of operation [11]. Another definition is that an electrically

small antenna fits inside a sphere with a radius

$$a < \frac{\lambda}{2\pi}, \tag{2.8}$$

where λ is the wavelength. A sphere with such a radius is referred to as the radian-sphere [13].

Electrically small antennas have some limitations. As a consequence of their electrically small size, they generally have a small radiation resistance, a high input reactance, low efficiency, low directivity, and narrow bandwidth [12]. Making an antenna electrically small is always a compromise between the size, efficiency and bandwidth, as all three cannot be optimized at once. The physical limits of the application often limit the antenna size and act as upper limits for the antenna performance.

Electrically small antennas are also difficult to measure using a cable connection, because the measurement cable can significantly affect the radiation properties of such an antenna. The measurements and their challenges are described more in Section 2.2.

2.1.4 Near and far field

The region around an antenna can be divided into the near and far fields. The near field can further be divided into reactive and radiating near fields. Fig. 2.2 illustrates this concept. The reactive near field is the region immediately surrounding the antenna. Reactive fields dominate in this region, meaning that the majority of the energy in the field oscillates back and forth between the electric and the magnetic fields in the vicinity of the antenna. This energy is not radiated. On the other hand, in the radiating near field the radiation fields dominate over the reactive fields.

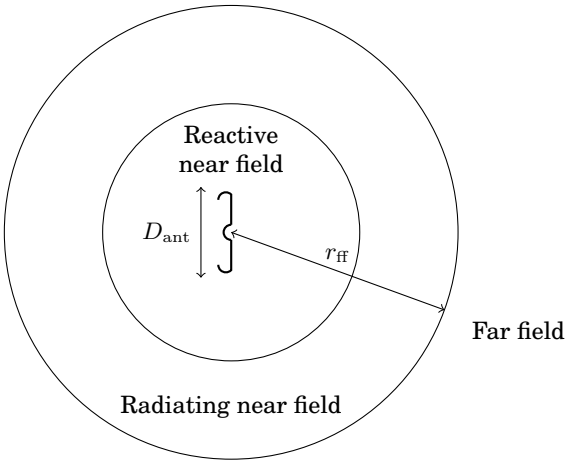

Fig. 2.2. The three regions surrounding an antenna.

The far-field region is the region where the angular field distribution of an antenna does not depend on the distance [11]. As a consequence, the antenna has a well-defined distance-independent *radiation pattern* in the far field. The radiation pattern is explained further in the following section. In the far field, the propagating wave can be approximated as a plane wave. The radiating wave is in reality a spherical wave, but it appears planar if the curvature of the sphere is large enough. In theory, this would only occur at infinite distance from the antenna, although in practice the difference is small enough at more reasonable distances.

Several conditions for the suitable distance can be defined [12], such as

$$r_{\mathrm{ff}} > \frac{2D_{\mathrm{ant}}^2}{\lambda}, \tag{2.9}$$

$$r_{\mathrm{ff}} > 5D_{\mathrm{ant}}, \tag{2.10}$$

$$r_{\mathrm{ff}} > 1.6\lambda, \tag{2.11}$$

where r_{ff} is the distance from the antenna, and D_{ant} is the largest dimension of the antenna. Depending on the electrical size of the antenna, different criteria can be the limiting factor. For electrically large antennas, (2.9) is often the defining criterion. The other conditions can be needed for electrically small antennas [12]. These limits are only approximate, as there is no exact transition between the regions.

2.1.5 Radiation pattern, directivity, and gain

It was mentioned in the previous section that an antenna has a distance-independent radiation pattern in the far field. The radiation pattern describes the relative radiated power to different directions from the antenna. An isotropic radiator would radiate all the power fed to it uniformly to all directions. Such a radiator, however, does not exist in reality. In practice, all antennas radiate more to certain directions. Some antennas radiate uniformly in one plane, and such antennas are called *omnidirectional*.

Directivity D of an antenna can be defined as the ratio of the radiation intensity in a given direction from the antenna to the radiation intensity averaged over all directions [11]. If no direction is specified, the directivity is assumed to refer to the direction of maximum radiation intensity.

A commonly used parameter related to directivity is *gain*

$$G = \eta_{\mathrm{rad}} D, \tag{2.12}$$

which can similarly be given as the maximum value or as a function of an angle. Additionally, *realized gain* can be defined by multiplying the gain with the impedance

mismatch factor η_{m}

$$G_{\mathrm{R}} = (1 - |\rho|^2)G = (1 - |\rho|^2)\eta_{\mathrm{rad}}D. \tag{2.13}$$

Realized gain therefore combines directivity, radiation efficiency and matching efficiency in one parameter. This can be beneficial if these quantities cannot be determined separately or for simply describing the antenna properties using only one parameter.

Gain (and directivity) is a power ratio and is often given in decibels. A commonly used unit for gain is dBi, which emphasizes that the gain value is referenced to an isotropic antenna with a gain of 1 (0 dB). An alternative unit dBd can also be used, which references the antenna gain to that of a half-wave dipole, 2.15 dBi. This representation is sometimes used at frequencies below 1 GHz, where a half-wave dipole is often used as a reference antenna [12].

2.1.6 Polarization

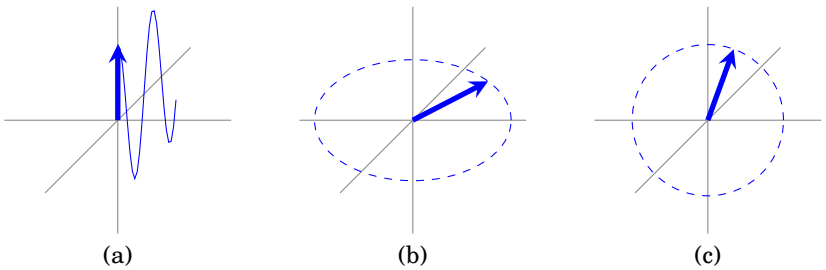

Fig. 2.3. The three antenna polarizations: (a) Linear (b) Elliptical (c) Circular.

The *polarization* of an antenna refers to the temporal behavior of the electric field vector of the radiating wave. It can be either linear, elliptical or circular. These three cases are illustrated in Fig. 2.3. In linear polarization, the electric field vector moves along a line. The electric field vector of a elliptically polarized wave rotates along an ellipse. Circular polarization is a special case of elliptical polarization, where the two axes of the ellipse are equal. One can define the *axial ratio* (AR) for elliptical polarization, describing the ratio between the different field components. The axial ratio can technically be defined for linear and circular polarizations as well, being infinite and one, respectively.

Circular and elliptical polarizations can be specified as right or left-handed. This refers to the rotation direction of the electric field. The electric field vector of a left-hand polarized wave rotates clockwise when observed from the direction to which the wave is traveling. A right-hand polarized wave rotates counterclockwise.

Polarization is important because the polarizations of the incoming wave and the receiving antenna must match. Otherwise some of the incoming power is lost. Circu-

lar polarization is often used with the reader antennas of transponder applications, because the orientation of the transponder can be arbitrary. With a linearly polarized reader antenna, the linearly polarized transponder could be oriented in such a way that the polarizations do not match. When two linearly polarized antennas are placed orthogonally to each other, all the power is lost due to polarization mismatch. With circular reader antenna polarization, however, the loss is at most 3 dB [12].

2.2 Measuring antenna properties

The use of electromagnetic simulation software has reduced the need for measurements during the design process. Instead of measuring several prototype iterations, the design process can be performed computationally. Nevertheless, measurements remain important for verifying the operation of the manufactured prototype or the finished device.

2.2.1 Impedance

The impedance of an antenna is usually the first characteristic to be measured [12]. This is because the impedance defines the operating bandwidth of the antenna, which is needed for measuring the other characteristics.

The impedance measurement of an antenna is usually performed using a VNA. The VNA gives the full impedance of the antenna, i.e. both the resistance and reactance. Obtaining the full impedance is preferable for better understanding of the antenna but obtaining only the magnitude of the reflection coefficient is in many cases adequate. The impedance of an antenna can change due to the environment, so the free-space operation of an antenna should ideally be measured in an anechoic chamber or in an absorber-lined box to minimize the effect of the surroundings [12]. Fig. 2.4 illustrates the impedance measurement.

A challenge with this method is that the measurement cable easily becomes a part of the radiating structure, especially if the AUT is electrically small. Measurement cables often carry unbalanced currents that can disturb the measuremenets. The effects of these currents can be reduced using ferrite chokes or a balun [14], but they do not solve the problem completely. An additional challenge with characterizing transponder antennas is that there usually is no connector where the measurement cable could be easily connected. Furthermore, the characteristic impedance of the VNA is typically 50 Ω, which is typically far from the actual load impedance of the

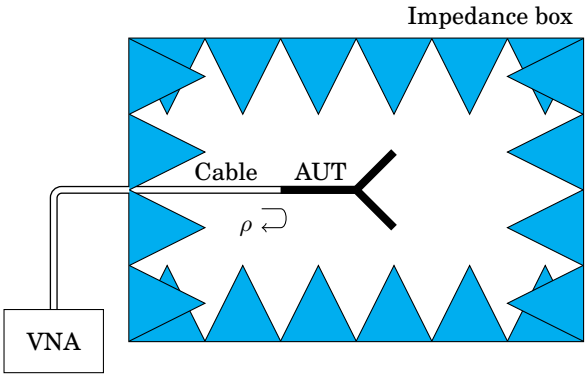

Fig. 2.4. Impedance measurement of an antenna.

transponder. Thus the measured reflection coefficient does not directly measure the operation of the transponder, but must be normalized to the actual load impedance.

2.2.2 Radiation pattern

The radiation properties of an antenna can also be measured. These include measuring the radiation pattern and the gain of the antenna. The radiation pattern measurements require a source antenna in addition to the AUT. The source antenna illuminates the antenna with a constant field. The AUT is rotated and the received power is recorded at different orientation angles. This is illustrated in Fig. 2.5. A two-axis rotator is needed to measure the full three-dimensional (3D) pattern, but radiation pattern cuts can be obtained using a two-dimensional turntable and by manually aligning the AUT along the proper axis.

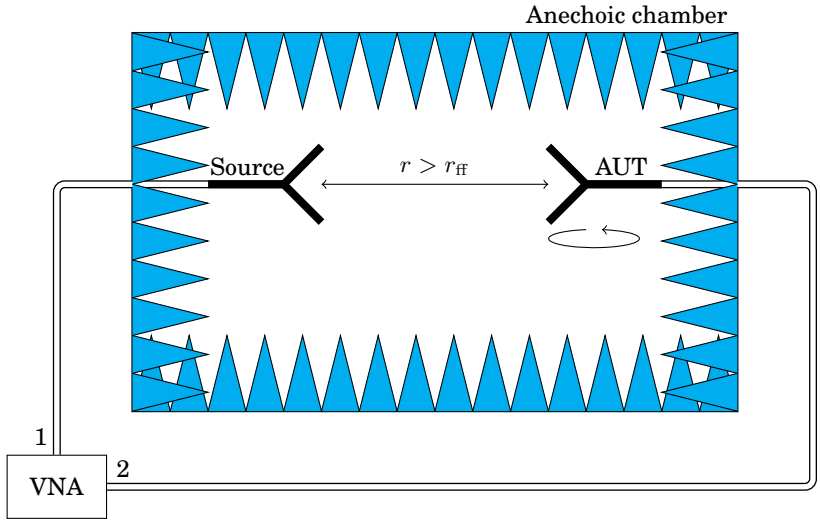

Fig. 2.5. Radiation pattern measurement of an antenna.

The measured radiation pattern is often normalized, meaning that the obtained values give the angular dependency of the radiation normalized to unity. In many

cases it is desirable to obtain the absolute level of radiation. One method for obtaining the directivity is to measure the radiation pattern in several planes. One can then integrate over this discrete 3D radiation pattern to obtain the maximum directivity. The gain can be obtained by estimating the radiation efficiency and using (2.12).

Alternatively, the gain can be measured using *gain comparison*. In this method, a reference antenna is used in addition to the AUT and the source antenna. The received power is measured using both the AUT and the reference antenna. The difference in received power is equal to the difference in the antenna gains. The gain of the reference antenna has to be well known. These antennas are often called *standard gain antennas*. Popular reference antennas include half-wave dipoles and pyramidal horn antennas.

These methods involve a cable connection to the AUT as well, so they have the aforementioned limitations when measuring small antennas. The added limitation is that the AUT must be rotated, so the positioning of the measurement cable must be considered.

2.2.3 Measurement of RFID transponders using a reader device

RFID transponders can be measured using a reader with variable transmit power. Such reader devices are commercially available, e.g., from Voyantic [8]. The measurement is performed by adjusting the transmit power of the reader device and checking for the response of the tag. An RFID chip has a specific sensitivity, i.e. the smallest power that activates the chip. The input power is then swept until the minimum power, at which the tag responds, is found. The read-out distance obtained with the maximum power can then be calculated from the sensitivity, minimum detectable power, and the measurement distance. This basic measurement does not give specific details about the operation of the antenna, but merely the maximum read-out distance of the whole transponder. This can be adequate in many cases as the read-out distance might interest the end user more than, e.g., the gain would. However, from an antenna characterization perspective, the information is not sufficient.

While these methods are useful for measuring RFID transponders, due to their reliance on the RFID principle, they are not usable for, e.g., harmonic transponders. They can be used for other antennas by manufacturing an RFID chip assembly and connecting it to the AUT [15].

2.2.4 Radar cross section measurement

When an antenna is illuminated with an electromagnetic wave, it scatters back some of the incoming wave. This is partly caused by the physical structure of the antenna and partly by the reflection from the load. By altering the load and measuring the backscattered response, it is possible to characterize the antenna. This backscattering-based measuremement technique is often referred to as the RCS measurement, as the backscattered response depends on the *radar cross section* (RCS) of the antenna [9].

The theory behind antenna backscattering was first investigated in [16]–[18]. Afterwards, this theory has been extended to characterizing antennas. Research was performed for, e.g., antenna gain [9]. Obtaining the antenna impedance of a resistively loaded antennas was first investigated [19] and the technique has recently been developed further for reactively loaded antennas [20]. This method has the advantage of not requiring a cable connection. It, however, requires that the antenna can be terminated with different loads. The measurement equipment must also be rather sensitive.

3. Modeling and characterization of nonlinear phenomena

The measurement method presented in this thesis relies on the nonlinear properties of the transponder. To properly analyze the response given by the measurement, it is essential to know the underlying effects of this phenomenon to understand how it affects the response. In this chapter, the definition and properties of nonlinearity are discussed. A short introduction on nonlinearity is given in Section 3.1. Nonlinearity causes several different phenomena. These are explained in this chapter, beginning with the small-signal model in Section 3.2 and followed by harmonic distortion and rectification in Section 3.3, and intermodulation distortion and mixing in Section 3.4. Some examples for the applications of these effects are also given.

3.1 Definition of nonlinearity

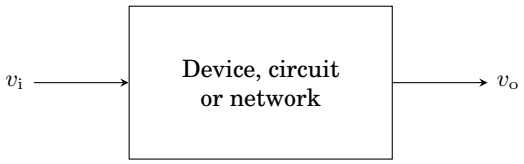

Fig. 3.1. A two-port network with an input signal v_i and output signal v_o. Adapted from [21].

Consider an element that, upon receiving an input signal v_i, generates an output signal v_o, as illustrated in Fig. 3.1. The element can be considered a component, a circuit or a device. The output of such an element is some function of the input,

$$v_\mathrm{o} = v_\mathrm{o}(v_\mathrm{i}). \tag{3.1}$$

The behavior of the element can be classsified as *linear* or *nonlinear*. For a linear device, the output follows the superposition principle

$$v_\mathrm{o}(av_1 + bv_2) = av_\mathrm{o}(v_1) + bv_\mathrm{o}(v_2), \tag{3.2}$$

where v_1 and v_2 are two input signals multiplied by constants a and b, respectively. It can be seen that the two input signals do not affect each other. Conversely, a nonlinear element is one that does not fulfill the condition in (3.2). The input signals become distorted due to nonlinearity, which produces several different nonlinear phenomena. These nonlinear models and phenomena are described in the following sections.

In practice, all realistic components are technically nonlinear because of noise at low signal levels [21]. However, in many cases they can be modeled as linear elements. There are also many elements whose operation is fundamentally based on nonlinearity, and therefore require nonlinear modeling and analysis. This modeling is discussed next.

3.2 Small-signal model

Modeling and analysis of nonlinear elements is in many cases rather laborious. The relation between the input and the output is seldom a easily solvable analytical function and analyzing the operation of the element might require iterative methods. It is often easier to linearize the equation, and to find a solution using linear analysis methods. One such method is the *small-signal approximation*, which is obtained by linearizing the element at some specific bias point, often referred to as the direct current (DC) operating point of the device.

A nonlinear function can be represented as a Taylor series

$$v_\mathrm{o} = f(v_\mathrm{i}) = a_0 + a_1 v_\mathrm{i} + a_2 v_\mathrm{i}^2 + + a_3 v_\mathrm{i}^3 + \ldots + a_n v_\mathrm{i}^n, \tag{3.3}$$

where a_n are the coefficients and $n \to \infty$. The coefficients are obtained from the derivatives of the nonlinear function

$$a_n = \frac{1}{n!} \frac{\mathrm{d}^n}{\mathrm{d}v_\mathrm{i}^n} v_\mathrm{o}(V_\mathrm{DC}), \tag{3.4}$$

where V_DC is the DC operating point of the element. The series cannot be calculated to include infinitely many terms due to practical reasons, but calculating a reasonable number of terms is in many cases sufficient.

The small-signal approximation is obtained by truncating the Taylor series, usually after the first two or three terms. A linear approximation is obtained by only including the first two. The output is therefore

$$v_\mathrm{o} \approx a_0 + a_1 v_\mathrm{i}. \tag{3.5}$$

An input signal with a DC and an alternating current (AC) signal component can be written as

$$v_\mathrm{i} = V_\mathrm{DC} + V_0 \cos(\omega t). \tag{3.6}$$

Substituting this input to (3.5) gives

$$v_\mathrm{o} = a_0 + a_1 V_0 \cos(\omega t). \tag{3.7}$$

This linear model approximates the output well if the input signal is reasonably small. As the input signal increases, the model becomes less accurate. Nevertheless, it is an useful model for nonlinear elements. The accuracy of the approximation can be increased by including higher-order terms. These terms also result in other nonlinear phenomena not considered in the first-order approximation, namely distortion, mixing, and rectification. These phenomena are analyzed in the following sections.

3.3 Harmonic distortion and rectification

Consider a sinusoidal input voltage with a fundamental frequency ω_0 and an amplitude of V_0

$$v_\mathrm{i} = V_0 \cos(\omega_0 t). \tag{3.8}$$

The output voltage is obtained from (3.3), this time including the higher order terms. Beginning with the second-order term $a_2 v_\mathrm{i}^2$ and using trigonometric identities, one obtains

$$a_2 \left(V_0 \cos(\omega_0 t)\right)^2 = \frac{a_2 V_0^2}{2} \left(1 - \cos(2\omega_0 t)\right), \tag{3.9}$$

from which it can be seen that the second-order term generates a signal at the second harmonic frequency $2\omega_0$ and also a constant term. The constant term results in the generation of a DC component. This process is known as *rectification*. Similar effect occurs for higher order terms, with terms $n = 3, 4, 5, \ldots$ producing harmonic frequency components at $3\omega_0 t, 4\omega_0 t, 5\omega_0 t, \ldots$. This results in a frequency spectrum shown in Fig. 3.2, with the first 5 harmonic components included. The actual magnitudes of the harmonic components depend on the coefficients a_n, which can be calculated from the nonlinear function. The strength of the harmonic components typically decrease as n increases, with the higher order components becoming negligibly small.

The rectifying effect of nonlinearity can be used to convert AC signals to DC. These rectifiers can be used to, e.g., convert the AC signal of a power grid to a suitable operating voltage for electronic devices. Diode detectors can be used to measure radio frequency (RF) power by measuring the rectified voltage. It is also an important factor in RFID, as the incoming RF signal is rectified to power the chip in the tag. This is discussed further in Section 4.1.

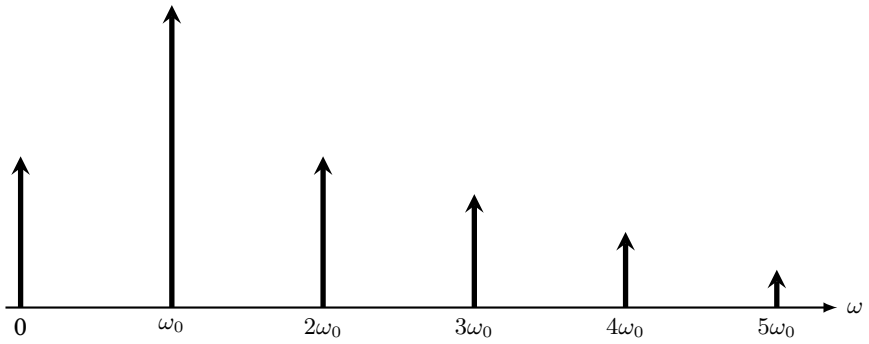

Fig. 3.2. The spectrum generated by a one-tone input signal in a nonlinear element. The amplitudes in the figure are arbitrary and depend on the nonlinear element.

The generation of the harmonic frequencies is known as *harmonic distortion*, which is generally unwanted. Because the harmonic frequency components are far away from the fundamental frequency, they are relatively easy to remove by filtering. Applications taking advantage of harmonic distortion include frequency multipliers, where the multiple of the frequency is generated via harmonic distortion. Harmonic transponders, as the name suggests, also use harmonic distortion for their operation. This is explained in more detail in Section 4.2.

3.4 Mixing and intermodulation distortion

Now consider a two-tone input signal, consisting of two different frequencies

$$v_{\mathrm{i}} = V_0 \left(\cos(\omega_1 t) + \cos(\omega_2 t)\right), \tag{3.10}$$

where ω_1 and ω_2 are the first and second fundamental frequencies. Here it is assumed that $\omega_2 > \omega_1$ and that their amplitudes V_0 are equal. Performing a similar analysis for the second-order term as in the previous section gives

$$a_2 V_0^2 \left(\cos^2(\omega_1 t) + 2\cos(\omega_1 t)\cos(\omega_2 t) + \cos^2(\omega_2 t)\right), \tag{3.11}$$

where the squared terms generate harmonics and DC, just like with the one-tone signal. However, there is also another term that is the product of both frequencies. With trigonometric identities, the product of the two frequencies becomes

$$2\cos(\omega_1 t)\cos(\omega_2 t) = \cos((\omega_2 - \omega_1)t) + \cos((\omega_1 + \omega_2)t). \tag{3.12}$$

This means that upon receiving two different input signals, a nonlinear element generates frequency components at the sum and difference frequencies, $\omega_1 + \omega_2$ and $\omega_2 - \omega_1$. This phenomenon is known as *mixing* and it is used in a wide range of

microwave systems to, e.g., convert the frequency between the lower-frequency baseband signal and the higher-frequency RF carrier signal. The elements performing this conversion are called mixers [21].

Similarly for the third-order term:

$$\begin{aligned} & a_3(V_0(\cos(\omega_1 t) + \cos(\omega_2 t)))^3 \\ & = \frac{a_3 V_0^3}{4}(9\cos(\omega_1 t) + \cos(3\omega_1 t) + 9\cos(\omega_2 t) + \cos(3\omega_2) + 3\cos((\omega_1 - 2\omega_2)t) \\ & + 3\cos((2\omega_1 - \omega_2)t) + 3\cos((\omega_2 + 2\omega_1)t) + 3\cos((2\omega_2 + \omega_1)t)) \end{aligned} \tag{3.13}$$

In addition to the third-order harmonics, there are also frequency components at $2\omega_1 - \omega_2$ and $2\omega_2 - \omega_1$, which are located at $|\omega_2 - \omega_1|$ away from the fundamental input frequencies. There are also terms at the fundamental frequencies. These are generally negative (due to the sign of a_3), meaning that they reduce the response at the fundamental frequencies [21]. This is known as *gain compression*. The generated spectrum up to the third order is illustrated in Fig. 3.3.

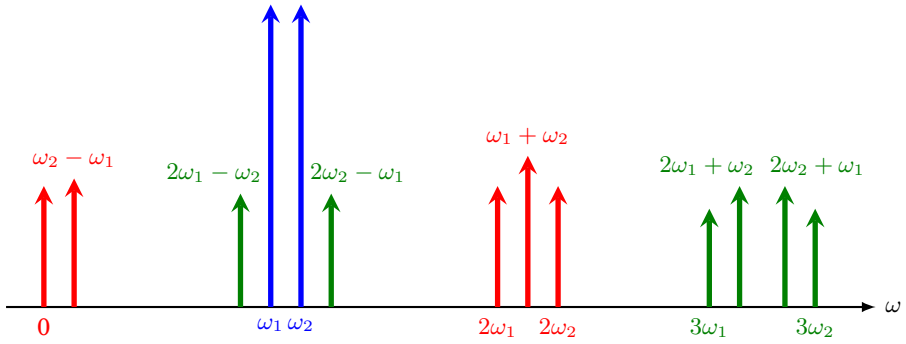

Fig. 3.3. The spectrum generated by a two-tone input signal in a nonlinear element. The first order frequency components are marked with blue, second-order with red, and third-order with green. Higher order terms are excluded.

By continuing the analysis for the higher-order terms, it can be found that the intermodulation distortion generates frequency components at $m\omega_1 + n\omega_2$, where $m, n = 0, \pm 1, \pm 2, \ldots$ The order of intermodulation can be defined as the sum of the absolute value of the coefficients $|m| + |n|$.

The third-order intermodulation products are of the most interest. In many applications, they are highly undesirable due to their proximity to the desired frequency components. This makes them difficult to remove by filtering. In the intermodulation measurement technique, however, the close proximity of the intermodulation frequencies actually makes the measurement possible. However, the intermodulation distortion generated by the measurement equipment is still a problem. These problems are explained later in Section 5.3.

Note that the different order terms have a different relation to the input voltage. The first order terms increase linearly with input voltage, second-order terms increase in second power, and so on. With small input voltages, the high order terms are very small. As the input voltage increases, the effect of higher order terms becomes more significant.

The *third-order intercept point* IP_3 is the hypothetical point where the linear and third-order frequency components are equal. The point can be referenced to the input power (IIP_3) or output power (OIP_3). In practice, the response compresses with high power levels, so the point is never reached. It can nevertheless be used to characterize the magnitude of the intermodulation distortion. Fig. 3.4 illustrates this concept. If the intercept point of a device is known, the magnitude of the third-order frequency components can be calculated from

$$P_{\text{out,IM}} = \frac{P_{\text{in}}^3}{OIP_3^2}, \tag{3.14}$$

where $P_{\text{out,IM}}$ is the output power at the intermodulation frequency, P_{in} is the input power of the nonlinear device, and OIP_3 is the third-order output intercept point of the device [21].

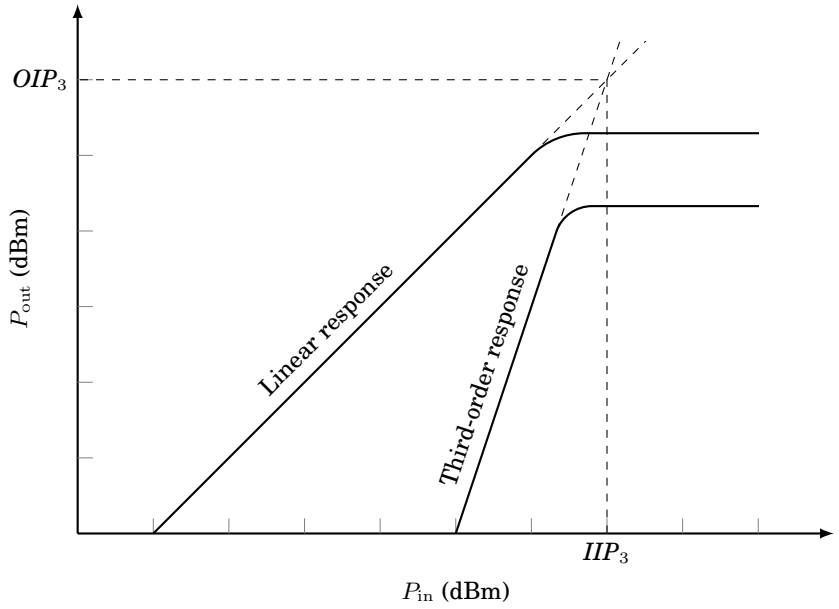

Fig. 3.4. The third-order intermodulation intercept point. Adapted from [21].

4. Transponders

A transponder is a device which, upon receiving a signal, transmits back another as a response. The name is a portmanteau of *trans*mitter and res*ponder*. Transponders can be divided into three different categories: active, semipassive and passive. Active transponders contain a powered transmitter and they generate a response using their own power supply. Such transponders can be found, e.g., in airplanes for identifying the aircraft. Semipassive transponders contain a power source for operating the circuitry, but the response is generated using the received signal. Passive transponders, on the other hand, contain no power source at all. They obtain all the required operating power from the received interrogation signal.

The passive functionality is obtained with nonlinear elements, which convert the received signal to suitable frequencies. In RFID, for example, the incoming RF signal is rectified to DC, which is required to operate the logic circuits in the RFID chip.

This thesis focuses mainly on passive transponders operating at microwave frequencies and involving nonlinear elements, i.e. the kinds of transponders the intermodulation measurement technique can be used for. RFID transponders and harmonic transponders are the most common examples, and will be the transponder types explained here.

4.1 RFID transponders

Radio frequency identification (RFID) can refer to many different systems, operating in different frequency bands and using different operation principles. These include, e.g., the modulated backscattering trandsponders, surface acoustic wave (SAW) transponders, and near-field communication (NFC). The operating frequency can range from 135 kHz to 5.8 GHz [1]. This frequency range can be divided into the low frequency (LF) 30–300 kHz, high frequency (HF) 3–300 MHz, and ultra-high frequency (UHF) 0.3–3 GHz bands. Different frequency bands have different applications. Lower frequency RFID is mainly used for close range systems, where the read-out distance is less than a meter. The advantage of the UHF transponders is their long read-out distance of several meters [1].

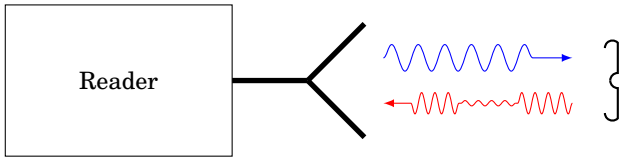

Fig. 4.1. RFID transponder utilizing the modulated backscattering principle.

For the purposes of this thesis, the main focus is on the RFID transponders operating in the UHF band and utilizing the modulated backscattering principle. This is due to their suitability for the intermodulation measurement technique. Such an RFID transponder (tag) consists of an antenna connected to an RFID chip. The chip is an integrated circuit containing all the elements necessary for the operation of the tag. The RFID chip requires DC voltage to operate, which is obtained by rectifying the incoming RF signal. There is a specific voltage level needed for the chip to operate, which then defines the amount of required power. From this, the maximum read range in the forward distance can be calculated.

The modulated backscattering principle is somewhat similar to the RCS measurement of Section 2.2.4. That is, the backscattered power of the antenna depends on the properties of the load. By adjusting the load resistance connected to the antenna, the reflected power can be changed. This change can be seen as the modulation of the backscattered signal [1]. Fig. 4.1 illustrates the operation of such an RFID transponder.

4.2 Harmonic transponders

A harmonic transponder operates by multiplying the incoming fundamental frequency and responding at a harmonic frequency. This enables detecting the target in cluttered environments where the reflections from the environment can obscure those from the target. This is illustrated in Fig. 4.2. The reader of a harmonic transponder system is generally referred to as radar and the system itself as harmonic radar.

In theory, any harmonic frequency could be used or even any mixing product, should a two-tone input signal be used. These were first investigated as a two-frequency secondary radar, a subset of which the harmonic radar could be considered [22]. In practice, the second harmonic frequency $2f_0$ is used for harmonic transponders. Intermodulation sensors [23]–[27] use two input signals and measure the intermodulation products, much like the measurement technique in this thesis.

The requirement of having two distinct, harmonically separated frequency bands is a problem as both frequency bands should be available for the use with the transpon-

der. This kind of operation is rather simple to create in theory. It is obtained by connecting a diode to an antenna. The diode, as a nonlinear element, produces the second harmonic frequency as in (3.9), which is then radiated back to the reader. The challenges arise in the proper design of the transponder. As was discussed in Section 2.1.1, the impedance matching between the antenna and the diode has a significant impact on the performance of the transponder. The transponder antenna must be designed in such a way that it is matched at the received fundamental frequency and at the transmitted second harmonic frequency. This matching is usually obtained directly from modifying the antenna geometry. For research on the transponder antenna design, see, [28]–[30].

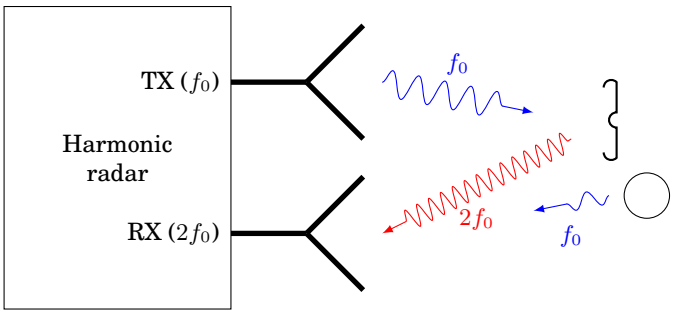

Fig. 4.2. Concept of a harmonic radar and transponder. The radar transmits at a fundamental frequency f_0 and receives at the second harmonic frequency $2f_0$. Reflected signals at the fundamental frequency do not interfere with detecting the transponder.

Unlike RFID transponders, a harmonic transponder does not contain any readable information. They merely provide information about the presence of the transponder; whether it is in the interrogation zone of the reader or not. Similar applications are in theft-detection systems, although those operate at much shorter distances [1].

First applications for harmonic transponders involved their use for a clutter-free automotive radar [4]. Later, their suitability for insect tracking was investigated [6], and they have subsequently been used to successfully track several kinds of insects [31]–[34] and small amphibians [35]. Such small targets can otherwise be difficult to separate from the environmental clutter. The simple construction of harmonic transponders makes it possible to manufacture them small enough to attach to an insect without significantly inhibiting its movement.

Harmonic transponders are also used to locate people buried under snow in the case of an avalanche [5]. Although their detection range is less than that of active avalanche beacons, their advantage is the passive operation. Users might forget to turn on their avalanche beacon or it might run out of battery, making it useless. A harmonic transponder acts as a sort of failsafe in these situations.

Additional components can be used to improve the operation of the transponder. One such component is an inductance in parallel to the diode. In addition to the second harmonic frequency, the transponder also produces higher order harmonic components and DC. A parallel inductance shorts the diode terminals at DC, so that the DC voltage across the diode remains zero. Without the parallel inductance, the rectified power would affect the operating point of the diode. The DC path also protects the diode from electrostatic discharge (ESD) [36]. The impedance matching of the transponder can also be done using additional components. A matching circuit can be created with capacitors and inductors, such as in the transponder in the introduction. Research on such transponders is still ongoing.

5. Intermodulation measurement technique

This chapter describes and analyzes the use of intermodulation response for characterizing antennas. The content of this chapter is the main outcome of this thesis work. It is mostly based on the content of [37], written by the author of this thesis. The thesis explains the contents of the article in more detail, based on the background information provided in Chapters 2 and 3.

The basic principle behind the technique is described in Section 5.1. The measurement of a harmonic transponder is then analyzed in detail, and the theoretical intermodulation response is derived in Section 5.2. Practical limitations of the model are then discussed in Section 5.3. The measurement can be performed using different arrangements of the measurement antennas. These different measurement geometries are compared in Section 5.4. The measurement technique can also be used to obtain the resonant frequencies and the impedance matching of the transponder. This is discussed in Section 5.5.

5.1 Background

The intermodulation measurement technique was first introduced in [10], where it was used to measure the normalized radiation pattern of a UHF RFID transponder. It exploits the nonlinear properties of the transponder. In the measurement, the transponder under test is illuminated with two closely-spaced frequencies f_1 and f_2. As was explained in Chapter 3, a nonlinear element generates intermodulation products at several frequencies. Of these frequencies, two are closely located to the fundamental frequencies, namely $2f_1-f_2$ and $2f_2-f_1$. This was illustrated in Fig. 3.3. Either of these frequency components can then be recorded. The recorded response depends on the characteristics of the antenna and can therefore be used to measure these characteristics. If the difference between the fundamental frequencies is small, it can be approximated that $f_1 \approx f_2 \approx 2f_1 - f_2 \approx 2f_2 - f_1$. Because all the frequencies are closely located, the intermodulation response can be approximated to depend on the antenna characteristics at one frequency only.

The advantage of this method is that it requires no cable connection to the antenna. The transponder is also measured with the actual load attached, so the results are representative of the operation of the transponder in the real application. The measurement can also be performed while the transponder is attached to an object, to see the effect it may have on the performance of the transponder.

5.2 Intermodulation response of a transponder

To properly take advantage of the intermodulation response for characterizing the antenna, the relation between the response and different parameters must be solved. Consider a transponder illuminated by a transmitter system. The incoming RF signal generates an intermodulation response in the transponder, which is then recorded by the receiver system. Starting from the transmitter, the power transmitted to the transponder at one frequency can be obtained from the Friis transmission equation [12]

$$P_{\mathrm{in}} = P_{\mathrm{t}} G_{\mathrm{t}} G_{\mathrm{tag}} \left(\frac{\lambda}{4\pi r_{\mathrm{t}}} \right)^2, \tag{5.1}$$

where P_{in} is the power received by the transponder and P_{t} is the input power of the transmitter. The gain of the transmitter $G_{\mathrm{t}} = G_{\mathrm{tc}} G_{\mathrm{ta}}$ consists of the gain of the transmitter chain (amplifiers, cables, etc.) G_{tc} and that of the transmitter antenna G_{ta}. G_{tag} is the gain of the transponder antenna, $\lambda = c/f$ is the wavelength, where c is the speed of light and f is the frequency, and r_{t} is the distance between the transmitter and the transponder. The offset $f_2 - f_1$ is assumed to be small, such that $f_1 \approx f_2$ and the transmitted power is approximately equal at both frequencies. The equation assumes free space propagation in the far field, so the distance between the transmitter and the transponder r_{t} should be larger than the far-field distance r_{ff}.

Next, the output power of the transponder at the intermodulation frequency is calculated. The antenna and the possible matching circuit is modelled as a Thévenin equivalent circuit, as was discussed in Section 2.1.1. The antenna resistance R_{A} is not separated into radiation and loss resistances R_{rad} and R_{loss}, as the measurement cannot obtain the efficiency. The effect of the efficiency is included in the gain G_{tag}. The equations derived here assume that the device is a harmonic transponder, meaning that the nonlinear element used is a Schottky diode. The diode is modeled using the small-signal model provided by the manufacturer of the diode used in the experiments [38]. The small-signal model includes a series inductance L_{s}, a parasitic capacitance C_{p}, a series resistance R_{s}, a small-signal junction resistance R_{j}, and a small-signal junction capacitance C_{j0}. The junction resistance is obtained from

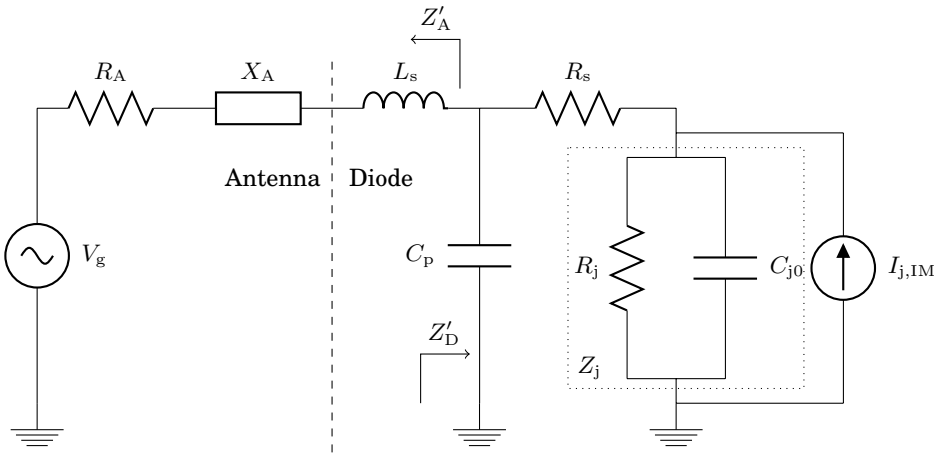

Fig. 5.1. Circuit model for a harmonic transponder consisting of an antenna (and possible matching circuit) connected to a Schottky diode.

$R_{\mathrm{j}} = 1/\alpha I_{\mathrm{s}}$, where I_{s} the saturation current and $\alpha = q/nkT$ where q is the elementary charge, n is an ideality factor, k is the Boltzmann constant and T is the temperature. To simplify the equations, the junction resistance and capacitance are represented as the junction impedance $Z_{\mathrm{j}} = (1/R_{\mathrm{j}} + \jmath\omega C_{\mathrm{j0}})^{-1}$. The combined circuit model for the transponder is illustrated in Fig. 5.1. The following equations can easily be modified for other nonlinear elements than the Schottky diode as well, assuming their circuit model is known.

The power P_{in} generates a voltage in the antenna. Assuming that the input power is equal at both fundamental frequencies, the voltage generated by the antenna is

$$V_{\mathrm{g}} = 2\sqrt{2R_{\mathrm{A}}P_{\mathrm{in}}}(\sin(\omega_1 t) + \sin(\omega_2 t)). \tag{5.2}$$

The current generated by the diode depends on the voltage across the diode junction V_{j}. Said voltage is obtained using the voltage division rule twice. First, over the antenna and the diode, and then over the series resistance and the junction of the diode. The junction voltage is

$$V_{\mathrm{j}} = \frac{Z'_{\mathrm{D}}}{Z'_{\mathrm{A}} + Z'_{\mathrm{D}}} \frac{Z_{\mathrm{j}}}{R_{\mathrm{s}} + Z_{\mathrm{j}}} V_{\mathrm{g}} = \hat{V}_{\mathrm{j}}(\sin(\omega_1 t) + \sin(\omega_2 t)), \tag{5.3}$$

where $Z'_{\mathrm{D}} = \left(\jmath\omega C_{\mathrm{p}} + (R_{\mathrm{s}} + Z_{\mathrm{j}})^{-1}\right)^{-1}$ and $Z'_{\mathrm{A}} = R_{\mathrm{A}} + \jmath X_{\mathrm{A}} + \jmath\omega L_{\mathrm{s}}$. The series inductance is included in the antenna impedance Z'_{A} to simplify the voltage calculation. The junction current generated by this voltage is [28]

$$I_{\mathrm{j}}(V_{\mathrm{j}}) = I_{\mathrm{s}}(e^{\alpha V_{\mathrm{j}}} - 1) + \frac{\mathrm{d}}{\mathrm{d}t}\left\{\frac{\Phi C_{\mathrm{j0}}}{1-\gamma}\left(1 - \frac{V_{\mathrm{j}}}{\Phi}\right)^{-\gamma+1}\right\}, \tag{5.4}$$

where Φ is the junction potential and γ is a profile parameter. This current can be represented as a current source parallel to the junction, as shown in Fig. 5.1.

The function for the current is nonlinear and therefore generates the phenomena discussed in Chapter 3. For the purposes of this measurement, the third-order intermodulation products are the most interesting ones. They are obtained from the third-order term of the Taylor approximation, as was shown in (3.13). The first three terms of the series are

$$I_\mathrm{j}(V_\mathrm{j}) \approx \frac{V_\mathrm{j}}{R_\mathrm{j}} - C_\mathrm{j0}\frac{\mathrm{d}}{\mathrm{dt}}\{V_\mathrm{j}\} + \frac{\alpha V_\mathrm{j}^2}{2R_\mathrm{j}} - \frac{C_\mathrm{j0}\gamma}{2\Phi}\frac{\mathrm{d}}{\mathrm{dt}}\{V_\mathrm{j}^2\} + \frac{\alpha^2}{6R_\mathrm{j}}V_\mathrm{j}^3 - \frac{C_\mathrm{j0}\gamma(\gamma+1)}{6\Phi^2}\frac{\mathrm{d}}{\mathrm{dt}}\{V_\mathrm{j}^3\}. \quad (5.5)$$

The first and second order terms can be ignored for purposes of the intermodulation response. The current at the intermodulation frequency is proportional to the third power of the junction voltage. Calculating this gives

$$(\hat{V_\mathrm{j}}(\sin(\omega_1 t) + \sin(\omega_2 t)))^3 = \frac{3}{4}\hat{V_\mathrm{j}}^3(\sin((2\omega_1 - \omega_2)t) + \sin((2\omega_2 - \omega_1)t)) + \ldots, \quad (5.6)$$

from which either intermodulation frequency can be chosen. For convenience, the selected frequency is further referred to using the subscript IM. The junction current at the intermodulation frequency is

$$I_\mathrm{j,IM} = \left(\frac{\alpha^2}{R_\mathrm{j}} - \jmath\frac{\omega C_\mathrm{j0}\gamma(\gamma+1)}{\Phi^2}\right)V_\mathrm{j}, \quad (5.7)$$

where the differentiation with respect to time has been replaced with $\jmath\omega$, as the voltage is time-harmonic (sinusoidal). The analysis continues with the assumption that $f_1 \approx f_2 \approx f_\mathrm{IM}$ so that all frequency-dependent variables are equal at these frequencies. Using current division, the current through the antenna $I_\mathrm{a,IM}$ can be calculated, and this current can then be used to solve the radiated output power

$$P_\mathrm{out,IM} = \frac{1}{2}R_\mathrm{A}|I_\mathrm{A,IM}|^2 = 4\left|\frac{\alpha^2}{R_\mathrm{j}} - \jmath\frac{\omega C_\mathrm{j0}\gamma(\gamma+1)}{\Phi^2}\right|^2\left|\frac{Z_\mathrm{j}}{R_\mathrm{s}+Z_\mathrm{j}}\right|^8\left|\frac{Z'_\mathrm{D}}{Z'_\mathrm{A}+Z'_\mathrm{D}}\right|^8 R_\mathrm{A}^4 P_\mathrm{in}^3. \quad (5.8)$$

In addition to the diode parameters, the above equation contains parameters related to the antenna impedance. For characterizing the antenna, all the antenna parameters should be solved from the equation. To facilitate solving the matching between the antenna and the diode, the impedance mismatch factor of (2.3) can be used. From it, the relation

$$\frac{4R_\mathrm{A}R_\mathrm{D}}{|Z'_\mathrm{A}+Z'_\mathrm{D}|^2} = 1 - |S_{11}|^2 \quad (5.9)$$

is obtained, where R_D is the total resistance of the diode and S_{11} is the reflection coefficient between the antenna and the diode. By substituting (5.9) into (5.8) the output power becomes

$$\begin{aligned} P_\mathrm{out,IM} =& \frac{1}{64R_\mathrm{D}^4}\left|\frac{\alpha^2}{R_\mathrm{j}} - \jmath\frac{\omega C_\mathrm{j0}\gamma(\gamma+1)}{\Phi^2}\right|^2\left|\frac{Z_\mathrm{j}}{R_\mathrm{s}+Z_\mathrm{j}}Z'_\mathrm{D}\right|^8(1-|S_{11}|^2)^4 P_\mathrm{in}^3 \\ =& E_\mathrm{IM}(1-|S_{11}|^2)^4 P_\mathrm{in}^3, \end{aligned} \quad (5.10)$$

where the intermodulation properties of the diode are denoted with E_{IM}. The intermodulation response at the receiver can then be calculated by using the Friis transmission equation. The received response is

$$P_{\mathrm{r,IM}} = \underbrace{P_{\mathrm{t}}^3 \frac{G_{\mathrm{t}}^3 G_{\mathrm{r}}}{r_{\mathrm{t}}^6 r_{\mathrm{r}}^2} \left(\frac{\lambda}{4\pi}\right)^8}_{\text{measurement setup}} \underbrace{G_{\mathrm{tag}}^4 (1 - |S_{11}|^2)^4}_{\text{realized gain of antenna}} \underbrace{E_{\mathrm{IM}}}_{\substack{\text{mixing} \\ \text{element}}} , \tag{5.11}$$

where G_{r} is the gain of the receiver antenna and r_{r} is the distance between the transponder and the receiver. This form clearly separates the three factors affecting the intermodulation response: measurement setup, antenna properties, and mixing element properties. The measurement setup and antenna parts are the same for any transponder. The mixing element properties change depending on the nonlinear load, which defines the value of E_{IM}.

5.3 Dynamic range of the measurement

The response calculated in (5.11) is the theoretical response. In practice the actual response follows the model only within a specific power range. The power range has both an upper and a lower limit. The ratio of the largest and smallest power where the model is valid is called the *dynamic range* of the measurement. This section focuses on the limiting factors of the measurement, their causes, and explains some methods for increasing the dynamic range. There are four factors that can limit the dynamic range of the measurement: input power, noise, transponder nonlinearity, and intermodulation distortion from the measurement equipment itself.

Noise is a fundamental limiting factor for all measurements. A receiver has a *noise floor*, consisting of the noise of the receiver and the environmental noise the receiver is recording. This sets a limit for the smallest signal a receiver can distinguish.

Just like the transponder, the measurement equipment contains nonlinear elements. These generate intermodulation products as well, which in some cases can obstruct the intermodulation response of the transponder. This intermodulation distortion can be generated both by the transmitter and the receiver part of the measurement setup. The distortion in the transmitter is caused by the two signal-generating parts at f_1 and f_2 not being completely isolated from each other, i.e. the signal at f_1 leaks to the instrument generating f_2 and vice versa. These two frequencies then mix, generating intermodulation distortion. The generated distortion then couples through the measurement antennas to the receiver. The distortion in the receiver is caused by the two input signals at f_1 and f_2 coupling to the receiver, and these signals then generate intermodulation products inside the receiver.

As these factors limit the dynamic range of the measurement method, their effect should be made as small as possible. The noise power is usually defined by the receiver and cannot be improved further. However, the intermodulation distortion can be minimized with proper design of the measurement setup. Considering both the noise and the intermodulation distortion, the total received power of the noise and the interference at the intermodulation frequency is

$$P_{\mathrm{NI}} = P_{\mathrm{N}} + \frac{|S_{21}|^2 P_{\mathrm{t}}^3}{LOIP_{3,\mathrm{t}}^2} + \frac{(P_{\mathrm{t}}|S_{21}|^2)^3}{L^3 OIP_{3,\mathrm{r}}^2}, \tag{5.12}$$

where P_{N} is the noise power, L is attenuation before the receiver, $|S_{21}|^2$ is the coupling between the transmitter and receiver antennas, and $OIP_{3,\mathrm{t}}$ and $OIP_{3,\mathrm{r}}$ are the third-order intercept points of the transmitter and the receiver.

Furthermore, *the signal-to-interference-plus-noise-ratio* (SINR) for the system can be defined. It is the ratio of the received response from the transponder $P_{\mathrm{r,IM}}$ and the received interference P_{NI}, in other words

$$\mathrm{SINR} = \frac{P_{\mathrm{r,IM}}/L}{P_{\mathrm{N}} + \frac{|S_{21}|^2 P_{\mathrm{t}}^3}{LOIP_{3,\mathrm{t}}^2} + \frac{(P_{\mathrm{t}}|S_{21}|^2)^3}{L^3 OIP_{3,\mathrm{r}}^2}}. \tag{5.13}$$

Note that the attenuation L reduces the received intermodulation response as well.

For the largest possible dynamic range, the SINR should be maximized. Equation (5.13) shows several ways this can be attained. The noise power and the intermodulation intercept points are defined by the measurement equipment. The OIP_3 of a transmitter can be increased by increasing the isolation between the two signal-generating paths, such as by adding isolators to the transmitter chain. After selecting the equipment, the main factors for increasing the SINR are the attenuation L and the coupling $|S_{21}|$. Of these, the coupling between the transmitter and receiver antennas should be minimized first, as it decreases distortion caused by both the transmitter and receiver without degrading the received response. This can be minimized with proper placement of the measurement antennas. If possible, absorbing material could also be placed between the antennas to decrease coupling.

The distortion can also be reduced by attenuating the received signal. However, the attenuation also reduces the received signal. It can be seen from (5.13) that the attenuation does not improve the ratio of the response and the transmitter-generated distortion, as they both are reduced at the same rate. However, the distortion generated by the receiver is reduced in the third power, so the attenuation improves the SINR if the receiver-generated distortion is the limiting factor.

The attenuation effectively increases the effect of the noise by the same amount and therefore should not be too large. The optimal attenuation is found by solving

the maximum of SINR as a function of L. The maximum is found by differentiating the SINR with respect to L and then solving the zero. The optimal attenuation is

$$L_{\mathrm{opt}} = P_{\mathrm{t}}|S_{21}|^2 \sqrt[3]{\frac{2}{P_{\mathrm{N}}\boldsymbol{OIP}_{3,\mathrm{r}}^2}}. \tag{5.14}$$

When $L = L_{\mathrm{opt}}$, the noise power is equal to the receiver-generated distortion, so their effect on the dynamic range is equal as well. With further attenuation the effect of the noise increases and the dynamic range actually begins to decrease. After adding the attenuation, it is also possible that the transmitter-generated distortion becomes the limiting factor instead.

The upper limit of the dynamic range can be defined either by the maximum input power or the small-signal region of the diode. The maximum input power can be limited by the equipment or frequency regulations.

The response was derived from the small-signal model of the diode. This model is only valid when the power received by the transponder is small. At higher power levels the junction resistance R_{j} of the diode changes due to self-biasing. Also, the small-signal approximation is less accurate when the AC voltage swing is large.

The power delivered to the transponder should therefore be kept constant to ensure that the transponder is operating under small-signal conditions during the whole measurement. The transponder response is not perfectly linear even under the small-signal conditions, so using constant delivered power should minimize the error caused by the model. This can be done by selecting a reference frequency f_{ref} and a corresponding input power P_{ref} where the model is valid. Changes in frequency, gain and matching can then be compensated by adjusting the input power to

$$P_{\mathrm{adj}} = \frac{P_{\mathrm{ref}} G_{\mathrm{tag,ref}}(1 - |S_{11,\mathrm{ref}}|^2)}{G_{\mathrm{tag}}(1 - |S_{11}|^2)} \left(\frac{f}{f_{\mathrm{ref}}}\right)^2, \tag{5.15}$$

where P_{adj} is the adjusted input power and $G_{\mathrm{tag,ref}}$ and $S_{11,\mathrm{ref}}$ are the gain and reflection coefficient at the reference frequency. Initial impedance matching or radiation pattern calculations can be done using constant input power, and the input power can be adjusted in the next measurement based on these initial results. This process can be repeated, iterating multiple times until the calculated values remain constant between iterations.

The power compensation simplifies for gain measurements. When measuring the gain or the radiation pattern, the frequency and the mismatch loss remain constant. Because of this, (5.15) simplifies to

$$P_{\mathrm{adj}} = P_{\mathrm{ref}} \frac{G_{\mathrm{tag,ref}}}{G_{\mathrm{tag}}}. \tag{5.16}$$

Based on these limitations, the dynamic range for the measurement can be defined. The upper limit of the dynamic range can be caused by the maximum obtainable response $P_{\mathrm{r,max}}$ or the maximum response $P_{\mathrm{r,ss}}$, where the small-signal model is still valid. The minimum limit is caused by the noise and interference power P_{NI} plus some $\mathrm{SINR}_{\mathrm{min}}$ to ensure the interference does not significantly add up (constructively or destructively) to the response. The dynamic range is illustrated in Fig. 5.2. Note that either $P_{\mathrm{t,ss}}$ or $P_{\mathrm{t,max}}$ can be the limiting factor.

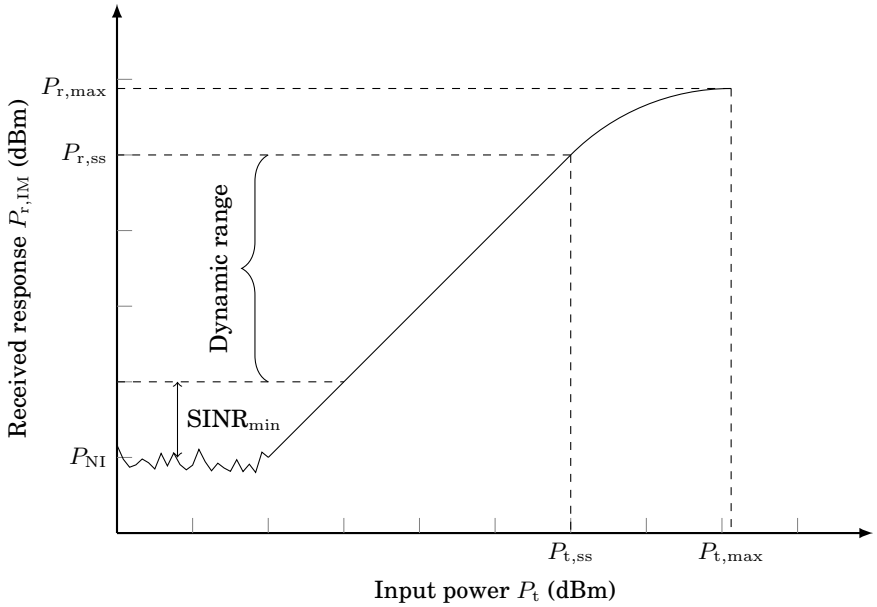

Fig. 5.2. An illustration of the dynamic range of the intermodulation measurement.

5.4 Radiation pattern measurement geometries

The positioning of the measurement antennas should be considered in the measurement. It is especially important when the radiation pattern of the transponder is measured. In this section, three potential measurement geometries are introduced. Their advantages and disadvantages are compared. The different geometries result in different response, so equations are presented to solve the radiation pattern from the measured response.

The calculated intermodulation response in (5.11) depends on the realized gain of the transponder antenna. For the purposes of the following equations, the realized gain of the transponder $G_{\mathrm{R,tag}}$ is denoted with $G(\theta, \phi) = G(\Omega)$, where Ω is the transponder orientation angle consisting of θ and ϕ, the polar and azimuthal angles in spherical coordinates. The response is proportional to $G(\Omega_{\mathrm{T}})^3 G(\Omega_{\mathrm{R}})$, where the subscripts T and R refer to the angular orientation of the transponder with respect

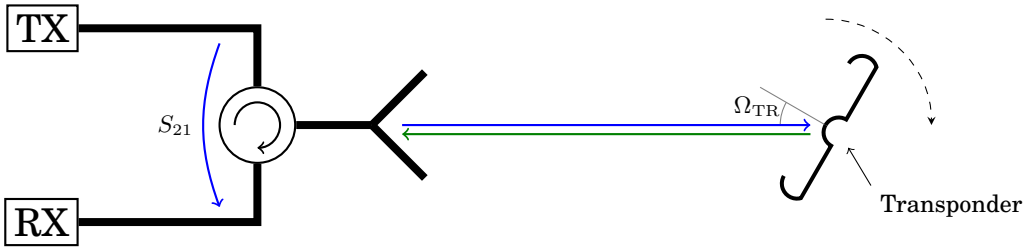

Fig. 5.3. Monostatic geometry.

to the transmitter and the receiver antennas. Solving the realized gain from (5.11) gives

$$G(\Omega_{\mathrm{T}})^3 G(\Omega_{\mathrm{R}}) = \left(\frac{4\pi}{\lambda}\right)^8 \frac{r_{\mathrm{t}}^6 r_{\mathrm{r}}^2}{G_{\mathrm{t}}^3 G_{\mathrm{r}} E_{\mathrm{IM}} P_{\mathrm{t}}^3} P_{\mathrm{r,IM}} = A P_{\mathrm{r,IM}}, \tag{5.17}$$

where all angle-independent (constant) terms in the equation are combined under A to shorten further equations. Obtaining the absolute gain pattern requires that all the parameters contained within A are known precisely. If this is not the case, only a normalized radiation pattern can be obtained.

With the relation between the realized gain and the intermodulation response solved, the next part is to consider the actual measurement geometry used. Different measurement geometries have different advantages and disadvantages. In this thesis, three alternate measurement geometries are considered. The geometries considered are monostatic, bistatic, and multistatic. These are described and compared in the following sections.

5.4.1 Monostatic measurement

In monostatic geometry, the transmitter and the receiver are located in the same position, as illustrated in Fig. 5.3. In practice, this is obtained using only one measurement antenna, and separating the transmitter and receiver paths with a circulator. With only one measurement antenna the transponder orientation is the same towards both the transmitter and the receiver, i.e. $\Omega_{\mathrm{R}} = \Omega_{\mathrm{T}}$. Denoting this angle with Ω_{TR} and solving the gain from (5.17) gives

$$G(\Omega_{\mathrm{TR}}) = \sqrt[4]{A P_{\mathrm{r,IM}}(\Omega_{\mathrm{TR}})}, \tag{5.18}$$

where $P_{\mathrm{r,IM}}(\Omega_{\mathrm{TR}})$ is the measured response when the transponder is aligned towards Ω_{TR}.

The advantage of this method is that it requires only one antenna. Additionally, the gain at each point requires only the measurement at the same point. Unlike in the other geometries, the coupling $|S_{21}|$ between the transmitter and the receiver cannot

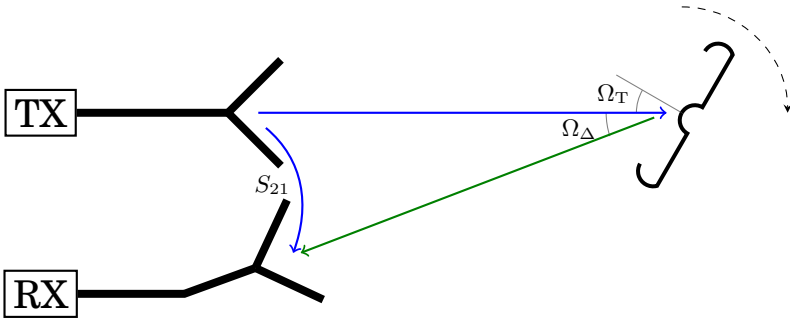

Fig. 5.4. Bistatic geometry.

be changed by adjusting the antenna placement. Instead, the coupling is defined by the isolation of the circulator, which can be less than that of two physically separated antennas. If the isolation is not adequate, the coupling can result in significant distortion, limiting the dynamic range. Another drawback is that the response is proportional to G^4. The measured gain therefore significantly affects the measured response, requiring large dynamic range. These limitations can make distinguishing the radiation pattern minima difficult with this geometry.

5.4.2 Bistatic measurement

Two separate measurement antennas are used in the bistatic measurement. In the measurement, both antennas remain stationary while the transponder is rotated. Fig. 5.4 illustrates this geometry. The measurement antennas must be aligned along the same plane as the rotation of the transponder. The measured power as a function of transponder gain is

$$G(\Omega_\mathrm{T})^3 G(\Omega_\mathrm{T} + \Omega_\Delta) = A P_{\mathrm{r,IM}}(\Omega_\mathrm{T}). \tag{5.19}$$

where $\Omega_\Delta = \Omega_\mathrm{R} - \Omega_\mathrm{T}$ is the offset between the transmitter and the receiver on the rotation plane. Now the response depends on the transponder gain at two different angles. This means that the gain cannot be calculated from only one measurement point, but at least two points need to be measured in order to solve the gain even in one point. The offset Ω_Δ should be equal to or a multiple of the angular step in the measurement so that when the transponder is rotated, the same measurement points align with both the transmitter and the receiver. If the full circle is measured with n measurements the gain can be solved at n points $G_1, \ldots, G_n$. Using this discrete notation, (5.19) can be modified to

$$3G_i + G_{i+\Delta} = A + P_{\mathrm{r},i} \tag{5.20}$$

where all quantities are in decibels and i and Δ are the angles in angular steps

$$i = \frac{\Omega_{\mathrm{T}}}{360^\circ} n \tag{5.21}$$

and

$$\Delta = \frac{\Omega_{\Delta}}{360^\circ} n. \tag{5.22}$$

The indices are cyclic, so that, e.g., $G_{n+1} = G_1$. With n measurements and variables a linear system of equations can be formed, represented using an n-by-n matrix

$$\begin{pmatrix} 3 & \cdots & 1 & \cdots & 0 \\ 0 & 3 & \cdots & 1 & \vdots \\ \ddots & \ddots & \ddots & \ddots & \ddots \\ \vdots & 1 & \ddots & 3 & 0 \\ 0 & \cdots & 1 & \cdots & 3 \end{pmatrix} \begin{pmatrix} G_1 \\ G_2 \\ \vdots \\ G_{n-1} \\ G_n \end{pmatrix} = \begin{pmatrix} A + P_{\mathrm{r,1}} \\ A + P_{\mathrm{r,2}} \\ \vdots \\ A + P_{\mathrm{r,n-1}} \\ A + P_{\mathrm{r,n}} \end{pmatrix}. \tag{5.23}$$

The gain can then be solved by inverting the coefficient matrix and multiplying both sides of the equation by the inverse matrix. The gain thus becomes

$$\begin{pmatrix} G_1 \\ G_2 \\ \vdots \\ G_{n-1} \\ G_n \end{pmatrix} = \begin{pmatrix} 3 & \cdots & 1 & \cdots & 0 \\ 0 & 3 & \cdots & 1 & \vdots \\ \ddots & \ddots & \ddots & \ddots & \ddots \\ \vdots & 1 & \ddots & 3 & 0 \\ 0 & \cdots & 1 & \cdots & 3 \end{pmatrix}^{-1} \begin{pmatrix} A + P_{\mathrm{r,1}} \\ A + P_{\mathrm{r,2}} \\ \vdots \\ A + P_{\mathrm{r,n-1}} \\ A + P_{\mathrm{r,n}} \end{pmatrix}. \tag{5.24}$$

The gain calculation of the bistatic geometry does not specify any required offset. However, the practical limitations of the measurement technique result in a couple of considerations. First of all, the offset between the antennas affects the coupling from the transmitter to the receiver, as changing the offset changes the distance and the gain between the measurement antennas. An optimal location depends on the antennas and should be experimentally verified. Practical limitations caused by the limited space in the measurement area can also limit the placement of the antennas. Alternatively, the offset can be selected based on some *a priori* information of the radiation pattern of the measured transponder. The problem with the monostatic geometry was that when measuring a minimum of the radiation pattern, both the transmitter and the receiver are aligned towards the radiation pattern minimum, so the measured response is reduced significantly. With two antennas, one can be aligned towards a maximum when the other is aligned towards a minimum. This is possible for, e.g., a dipole as the maxima and minima of a dipole are separated from each other by 90°.

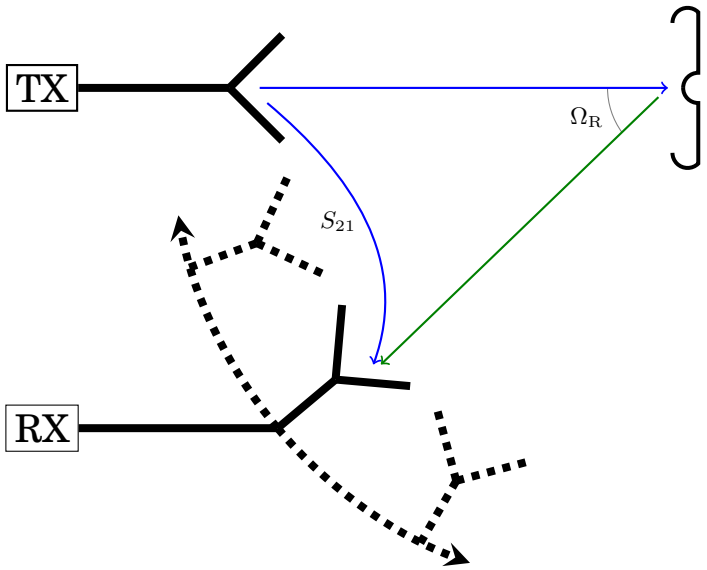

Fig. 5.5. Multistatic geometry.

In this geometry, the response is dependent on the gain at two different positions, which complicates the gain calculation. The gain can also be measured only in one plane at a time. Additionally, a limited dynamic range can cause further inaccuracies in the pattern even outside the minima.

5.4.3 Multistatic measurement

Multistatic geometry was used in [10], where the intermodulation measurement technique was introduced. In multistatic geometry, the transmitter and the transponder remain static relative to each other, while the response is measured from several different locations. As such, this would require several receiver antennas, but a more practical solution is to move one receiver antenna relative to the transmitter and the transponder. This means that the transmitter antenna should somehow be integrated with the turntable. Alternatively, the receiver antenna can be moved along a sphere with a constant radius. This is illustrated in Fig. 5.5.

With the multistatic geometry, the intermodulation response is directly proportional to the gain towards the receiver, and can be simply obtained from

$$G(\Omega_\mathrm{R}) = AP_\mathrm{r}(\Omega_\mathrm{R})/G(\Omega_\mathrm{T})^3. \tag{5.25}$$

As the transmitter and the transponder are static relative to each other, $G(\Omega_\mathrm{T})^3$ is constant. Thus, the normalized pattern is obtained directly from P_r. In order to solve the maximum gain, one measurement point should be selected such that $\Omega_\mathrm{T} = \Omega_\mathrm{R}$, in which case (5.18) can be used.

This geometry has several advantages over the two previous geometries. The transmitter can be positioned towards the maximum of the transponder radiation pattern. As the response is directly proportional to the gain, the required dynamic range is much smaller than in the other geometries. The input power of the transponder also remains constant, so there is no need for the use of the power compensation methods presented in Section 5.3.

The geometry does not directly give the absolute value of the measured gain. The transponder gain to the direction of the transmitter $G(\Omega_{\mathrm{T}})$ is assumed to be constant, but its value is not known. Obtaining the absolute gain requires placing the transmitter and the receiver in a monostatic position and using (5.18). Further limitations of the method occur in the mechanical operation. A turntable for only a small transponder is rather simple. However, this geometry requires that the measurement antennas are moved: either the transmitter antenna rotates alongside the transponder or the receiver antenna is moved along a sphere. This can be challenging, especially if the measurement antennas are physically large. If these mechanical requirements can be solved, the multistatic geometry is the best option for measuring the gain using the intermodulation measurement technique.

5.5 Resonance frequencies and impedance matching

In addition to the gain dependency, the intermodulation response also depends on the impedance matching between the antenna and the nonlinear mixing element. The resonance frequencies of the antenna appear as local maxima in the intermodulation response.

The magnitude of the reflection coefficient $|S_{11}|$ can be solved from (5.11), giving

$$|S_{11}|^2 = 1 - \sqrt[4]{\frac{r_{\mathrm{t}}^6 r_{\mathrm{r}}^2}{G_{\mathrm{tag}}^4 G_{\mathrm{t}}^3 G_{\mathrm{r}} E_{\mathrm{IM}}} \frac{P_{\mathrm{r,IM}}}{P_{\mathrm{t}}^3}} \left(\frac{4\pi}{\lambda}\right)^2 . \tag{5.26}$$

However, this assumes that the gain of the transponder G_{tag} is known at all measured frequencies. Simulations can provide a reasonable estimate.

Alternatively, one could instead solve the realized gain as a function of frequency. This requires no knowledge of the antenna parameters, as they are all combined under the realized gain. The realized gain can be obtained using the techniques and equations presented in Section 5.4 by sweeping the frequency instead of rotating the transponder.

The assumption in (5.11) was that the offset between the frequencies is small. If the offset is too large, there will be some error in the results due to the parameters

being different at each of the measurement frequencies. This is especially notable in the case of narrowband matching as the matching level can be significantly different at each of the frequencies.

Obtaining the complex antenna impedance is not possible using the current technique and equipment (see Chapter 6). For it to be obtainable, both the amplitude and the phase of the intermodulation response should be recorded. However, the equations were only derived for the power, meaning that the phase information was lost. This is because the laboratory equipment available for the experiments in Chapter 6 is not capable of recording the phase of the intermodulation response. The full impedance (or the complex reflection coefficient) cannot therefore be solved. Further development of the technique could involve research regarding the complex intermodulation response, provided that equipment for such measurements is available.

Obtaining only the magnitude of the reflection coefficient still provides important information, as it directly describes and relates to the operation of the transponder. One potential option for obtaining further information about the antenna impedance could be to fit an equivalent circuit model to the measured reflection coefficient. The obtained results are relatively reliable in the sense that they are obtained by terminating the antenna with the actual load used in the transponder. Thus the results apply directly to the transponder in the actual operation. This also enables the measurement to be performed while the transponder is attached to an object, to measure the effect of the object on the resonance frequencies and the radiation pattern [10].

6. Experiments

This chapter contains the experimental work of this thesis. Section 6.1 explains the measurement setup and the equipment used in the measurements. The measurement software is also described. The actual measurements and their results are described and discussed in Section 6.2, where a self-resonant harmonic transponder is used to validate the measurement technique presented in Chapter 5. Of the presented measurement geometries, bistatic geometry is selected for the measurements.

6.1 Measurement setup

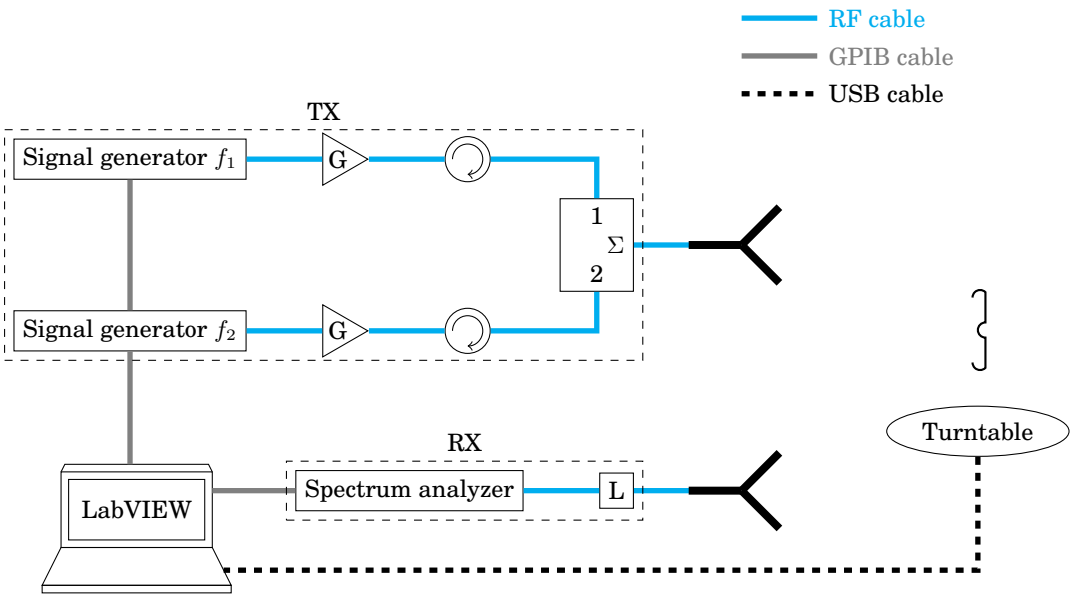

Fig. 6.1. Setup used in the measurements.

The measurement setup is similar to the one presented in [10], in which the technique was introduced. The setup is illustrated in Fig. 6.1, and it uses the following measurement equipment. The input signals are generated with two signal generators, Rohde & Schwarz SML-03 and SMT-06. Two Milmega AS0822-8L linear power amplifiers are used to amplify the signals generated by the signal generators. To reduce the transmitter-originated distortion, the isolation between the two signal sources is increased by adding two DITOM D3C0102S circulators before the power

combiner that connects both input signals to the transmitter antenna. Similar antennas are used for transmission and reception, those being ETS-Lindgren 3164-08 quad-ridged horn antennas. The receiver is an Anritsu MS2683A spectrum analyzer. The attenuation L in the measurement is caused by the losses in the measurement cables instead of an external attenuator. The gain and attenuation values at the two frequencies of interest are shown in Table 6.1. The measurement distance was selected to ensure far-field conditions at all measurement frequencies, while still keeping the distance short to reduce the free-space attenuation. The selected distance was 2 m.

Table 6.1. The parameters related to the measurement setup at the two main frequencies of interest.

Parameter	1 GHz	2 GHz
G_{tc}	29.79 dB	28.85 dB
G_{ta}	8 dBi	9.5 dBi
G_{r}	8 dBi	9.5 dBi
L	2.68 dB	3.34 dB

The frequency offset should be made as small as possible to make sure the single-frequency approximation is valid. It is found that this approach also has some practical limitations. With a too small offset, the measurement equipment produces spurious signals that occur close to the measured frequency. These signals can be picked up by the receiver and interfere with the measurement. A suitable offset was found to be 300 kHz, which can be considered small compared to the operating frequency and bandwidth.

A turntable is used for the radiation pattern measurements. The turntable is not capable of two-axis rotation, so the transponder under test must be aligned along the proper axis for rotation. The measured transponders and the transmitter and receiver horn antennas are linearly polarized. This requires adjusting the measurement antenna polarizations as well. Fig. 6.2 illustrates the measurement setup for these two pattern cuts. The turntable is a metallic structure, so it should be placed far from the transponder under test to ensure it does not affect the measured response.

The measurements are performed in an anechoic chamber to minimize the effect of reflections from the environment. The antennas are placed in a bistatic configuration, separated by 60°. The rest of the measurement equipment is placed in the control room of the chamber. Fig. 6.3 illustrates the measurement setup inside the chamber.

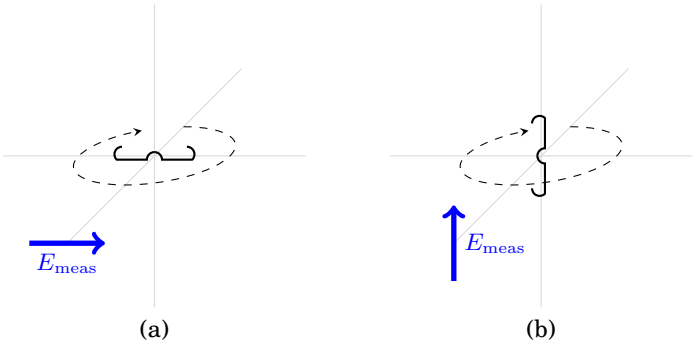

Fig. 6.2. Transponder alignment during the two radiation pattern measurements. Note the change in the polarization of the measurement antennas. The transponder antenna polarization is along the longer dimension. (a) *E*-plane measurement. (b) *H*-plane measurement.

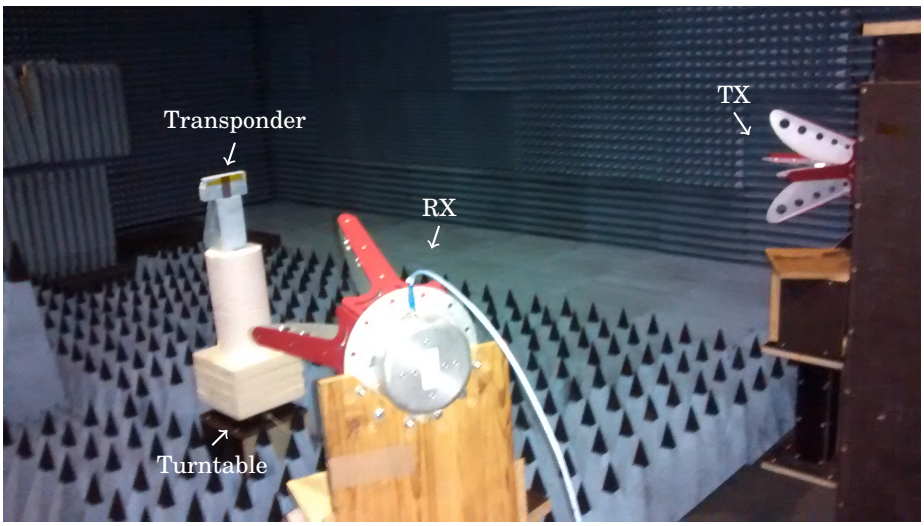

Fig. 6.3. Bistatic measurement setup in the anechoic chamber. The antennas are placed 2 meters from the transponder in a 60° angle.

6.1.1 Measurement software

For automated control and data collection, the measurement is controlled using a laptop which communicates with the measurement instruments via GPIB (General Purpose Interface Bus, IEEE-488) and USB (Universal Serial Bus). A measurement software was created with LabVIEW virtual instrumentation [39] by the author of this thesis. The purpose of the software is to change the measurement parameters, rotate the turntable, and record the measured response. Data processing is not included in the software, and it is performed using MATLAB [40] instead.

Potential future development for the software would be to include the data processing in the measurement software itself. In the current form, where the data processing is performed outside the measurement software, there is a need to measure several sets of data.

6.2 Harmonic transponder measurements

The results presented in Chapter 5 are validated by measuring a self-resonant harmonic transponder. This means that the matching is tuned with the antenna structure itself, without any matching circuit (with the exception of the zero-biasing inductor). The transponder operates at 1.014 and 2.028 GHz. The design of the antenna structure is explained in [29] and the harmonic response of the transponder has been investigated in [28], [30]. It was also the measured transponder in [37].

6.2.1 Intermodulation response and power dependency

The frequency of the signal generators and the spectrum analyzer is swept over the operating range of the measurement equipment of 0.8–2.2 GHz in 10-MHz increments. Increasing the frequency resolution records narrower changes but increases the measurement time. The frequency sweep is performed over different input power levels, ranging from -20 to 0 dBm in 1-dB increments.

Two of the measured responses are shown in Fig. 6.4. The comparison, the equivalent theoretical responses are calculated using (5.11) and the parameters listed in Tables 6.1 and 6.2. The antenna impedance and gain for the theoretical response are obtained from electromagnetic simulation software SEMCAD [41].

The response shows several important results. Comparing the measured and theoretical responses shows good agreement with some small differences. Looking at the case with smaller input power (red curve), the lower resonance frequency (1 GHz)

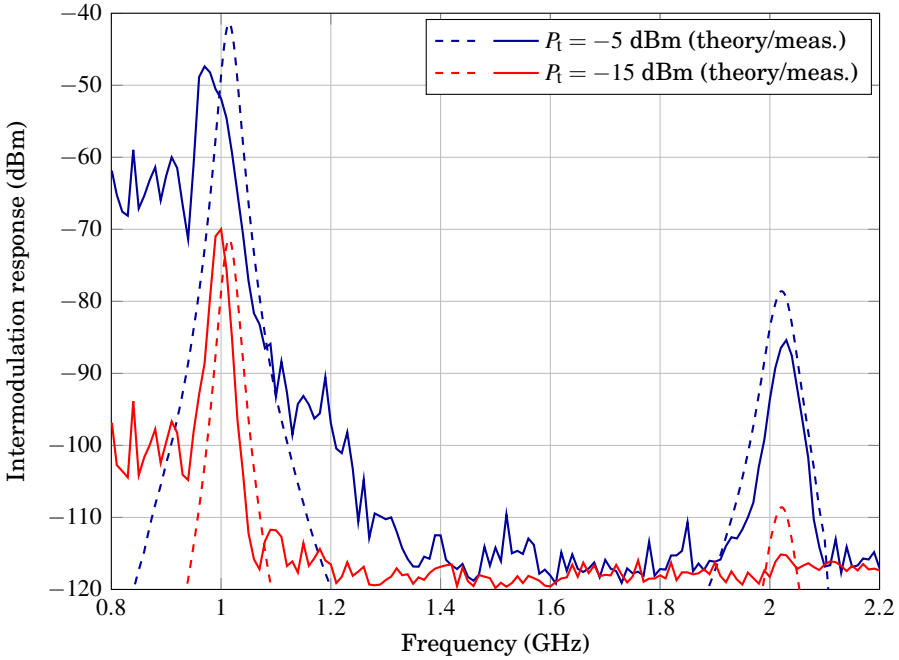

Fig. 6.4. The measured intermodulation response (solid lines) compared with the theoretical response (dashed lines) using two different input power levels.

Table 6.2. The diode parameters used for calculating the theoretical intermodulation response. Obtained from [38].

Parameter	Value
C_{j0}	2.25 pF
C_p	0.07 pF
I_s	10^{-14} A
L_s	0.7 nH
R_s	4.8 Ω
γ	1.4
Φ	3.5 V

has shifted slightly downwards from the theoretical one. The upper resonance frequency (2 GHz) should appear slightly above the noise floor, but there is no detectable response in the measurement. By increasing the input power by 10 dB (blue curve), several effects can be seen taking place. Firstly, the shape of the first resonance deforms, tuning the frequency of highest response to lower frequencies. This means that the power delivered to the diode is too large for the small-signal approximation to be accurate. The higher input power, however, enables detecting the upper resonance from the noise. The frequency of the resonance is close to what the theory and simulations predicted, although the level of the response is less than expected. This is easily explained by the difference in the impedance matching level. The results suggest that the manufactured transponder has somewhat worse impedance matching at the second resonance frequency.

Also apparent in the figure is the effect of the equipment-generated distortion. This distortion is picked up by the spectrum analyzer, appearing as an increased noise floor. The nominal operating frequency of the circulators used to separate the two signal generators is 1–2 GHz. At frequencies below 1 GHz, the isolation of the circulators degrades, causing more of the signal to leak through. This amplifies the generated intermodulation distortion in the transmitter.

The limitations of the small-signal model can be seen occurring at the first resonance with high input power. The shape and amplitude of the resonance are altered because small-signal conditions are no longer valid. At power levels where the first resonance is still in accordance with the model, the second resonance is not visible. Conversely, when the second resonance is well above the noise level, the model does not apply to the first resonance. This problem is notable for harmonic transponders that have two distinct frequency bands of interest but is absent in transponders operating only in one frequency band, such as conventional RFID tags. It should be noted that there is in practice no need to measure both frequency bands at the same time. The two resonance frequencies could also have been measured separately, possibly adjusting the setup (e.g. distance, attenuation) to better suit the measured frequency band.

Fig. 6.4 also shows a large difference in the magnitude of the response between the two resonance frequencies. It can be seen from (5.11) that the response is proportional to f^{-8}. By doubling the frequency, the response decreases by 24 dB due to this factor alone. This can be a problem when measuring antennas at higher frequencies. More directive measurement antennas might have to be used to obtain a large enough response.

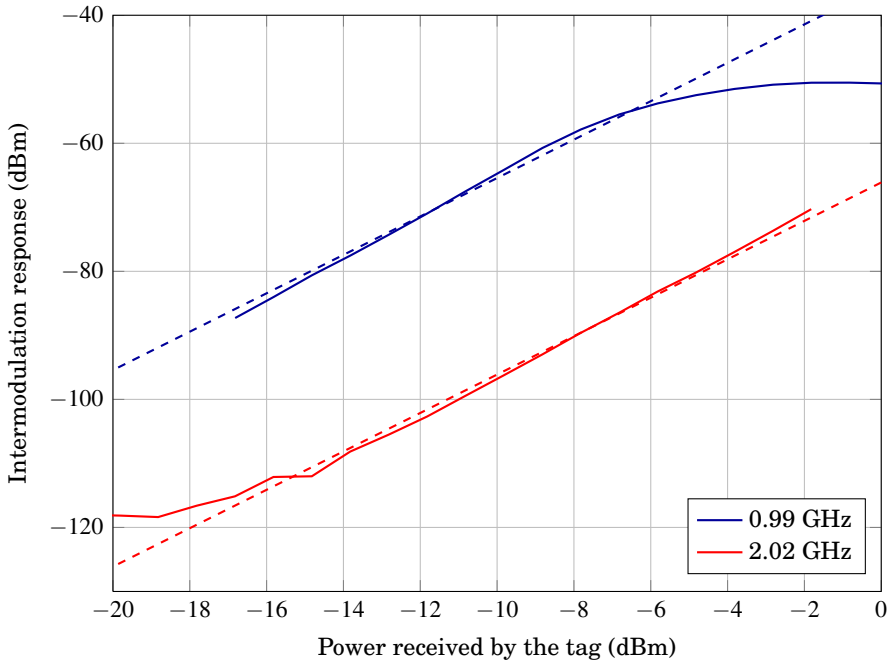

Fig. 6.5. Power dependency of the response at the two frequencies of best matching. The dashed lines represent the response predicted by the model when the matching is equal to that of the measurements.

To further demonstrate the effect of the input power, Fig. 6.5 illustrates the intermodulation response at two constant frequencies. Also the response calculated using (5.11) is given for reference. Because of the differences in the matching level between the simulated and real transponders, direct comparison would be difficult. Instead, the reflection coefficient calculated from the measurement is used. The calculation for this is shown later, in Section 6.2.3.

6.2.2 Gain measurement and validation of bistatic geometry

The realized gain of the transponder is measured at the first resonance frequency. The response is stronger at the first resonance, so the dynamic range in the measurement is larger. The radiation properties of a harmonic transponder are also more important at the fundamental frequency [28]. Bistatic geometry is selected for the measurement from the geometries presented in Section 5.4 as it is the most suitable for the available equipment. The measurement result also verifies the mathematically more complicated calculation in (5.19). Additionally, multistatic geometry has already been validated in [10].

The gain is measured in two pattern cuts, as was illustrated in Fig. 6.2. For both cuts, the offset between the antennas is selected to be 60°. The selected offset minimized the coupling between the transmitter and the receiver. It also prevents both

measurement antennas being aligned towards the radiation pattern minimum, as was discussed for the bistatic geometry in Section 5.4.2. When the measurement antennas are set to measure the E-plane pattern, the coupling causes transmitter-based distortion to leak to the receiver at the level of -115 dBm. This distortion cannot be reduced further so it acts as the noise floor for the E-plane measurement.

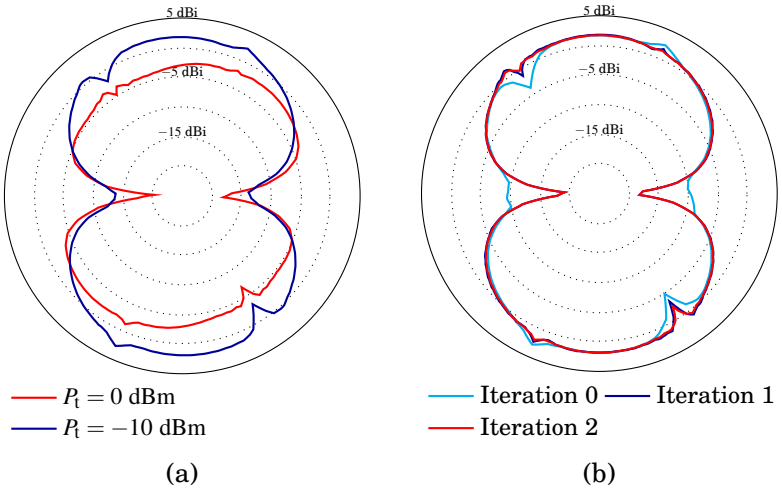

Fig. 6.6. Power dependency of the gain calculation.

The pattern is measured at several different power levels as there is no constant input power at which both the pattern minima and maxima are within the dynamic range. Fig. 6.6(a) illustrates this with the measured gain using two constant input powers, 0 and -10 dBm. Either the minima are obscured by noise (blue curve) or the small-signal model does not apply at the maxima (red curve).

To correct this problem, the gain is calculated iteratively. The gain is first measured using a constant input power of -15 dBm, and the input power is adjusted using (5.16) based on the measured gain. The gain is then calculated again from the results obtained using the adjusted input power. This can be performed multiple times until the pattern does not change between iterations. Fig. 6.6(b) illustrates the effect of the iterations. The first iteration already improves the result significantly. The second iteration has a minor effect on the result and further iterations do not have any meaningful effect.

The obtained pattern resembles that of a dipole antenna quite well. However, there is one problem with the result. There are noticeable errors in the pattern at angles offset by 60° from the minima (60°, 120°, 240°, and 300°). In the bistatic geometry, the gain at one point is calculated based on two measurement points. The other measurement point for the aforementioned gain angles is a minimum in the response.

A better SINR would fix this problem, but unfortunately that could not be obtained with the current measurement setup. Alternatively, the pattern could be measured

again with a different offset and then eliminating the erroneus results from the two results. This could be done by either moving the antennas to another angle or by swapping the cables connected to the transmitter and receiver antennas.

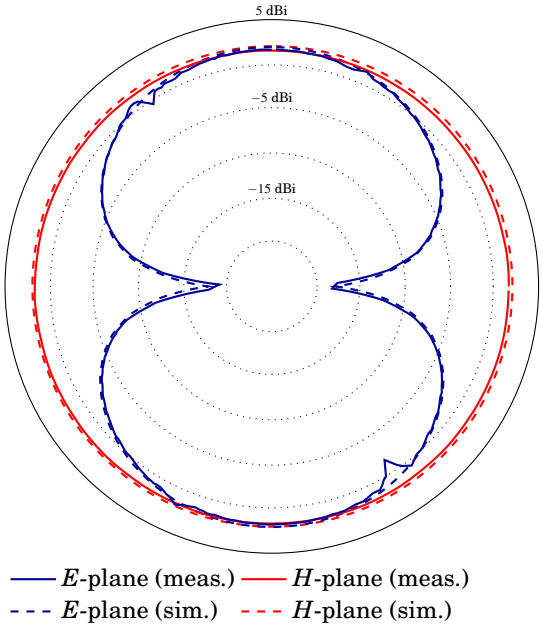

Fig. 6.7. Comparison of the patterns with the simulations.

After obtaining the E-plane cut, the H-plane cut was measured as well. The measurement antennas and the transponder were set to the configuration of Fig. 6.2(b). The transponder antenna is omnidirectional in this plane, so there are no problems caused by the limited dynamic range or pattern minima. Both measured gain patterns are then compared with patterns obtained from simulation software. The results are shown in Fig. 6.7. The measurements agree very well with the simulated patterns, with the exception of the errors in the E-plane caused by the low SINR.

6.2.3 Impedance matching

The frequency-dependent operation of the transponder could be represented using realized gain. Showing the reflection coefficient can be more illustrative. To calculate the reflection coefficient $|S_{11}|$ from (5.26), the gain of the transponder must be known. The gain is estimated using the results obtained from the electromagnetic simulations.

As was previously discussed, the dynamic range of the measurement is not sufficient for measuring both resonance frequencies with constant input power. The input power must therefore be adjusted to obtain correct results for both resonances.

The change in accepted power due to the differences in propagation is compensated using (5.15).

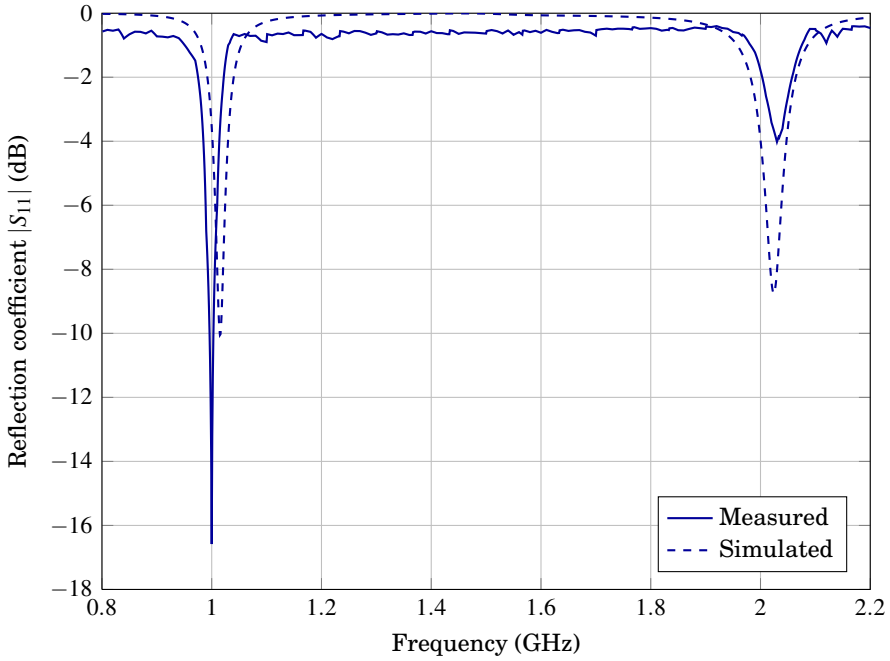

Fig. 6.8. Magnitude of the reflection coefficient for the measured harmonic transponder. The reflection coefficient is normalized to the diode impedance.

The measured reflection coefficient is illustrated in Fig. 6.8. The results suggest a slight detuning of the first resonance frequency and a larger reflection coefficient at the second resonance frequency. Otherwise the shape of the resonances is similar in both the simulations and the measurements. The intermodulation response itself, that was illustrated in Fig. 6.4, also showed those results. So in a sense the impedance matching calculation is not necessary for estimating the resonance frequencies. The matching calculation is useful for more detailed information regarding the level of the matching. The matching level outside the operating frequencies (e.g. at 1.5 GHz) appears to be better than in the simulations. This is because the noise floor acts as the “response” at those frequencies.

7. Summary and conclusions

In this master's thesis, the intermodulation measurement technique is analyzed. A theoretical model is derived for the intermodulation response of a harmonic transponder using the small-signal model of a Schottky diode. The derived model is then used to obtain the relation between the intermodulation response and the antenna characteristics. The obtained relation can be used to characterize antennas based on the measured intermodulation response.

Practical limitations of the model are considered. These are mainly due to the limited dynamic range of the measurement technique. Different sources for these limitations are presented. These include noise, interfering intermodulation distortion, input power, and the small-signal model of the diode. Techniques for reducing the effect of these limitations and therefore improving the dynamic range are discussed.

The measurement itself can be performed using several different physical arrangements of the measurement antennas and the transponder. Three potential measurement geometries are discussed in this thesis, namely the monostatic, bistatic, and multistatic geometries. Their advantages and disadvantages are compared.

The theoretical results of this thesis were validated by characterizing a harmonic transponder. The results showed good agreement between the theory and the measurement, and that the method is suitable for characterizing harmonic transponders. A challenge related to harmonic transponders was that there is a large difference between the intermodulation responses at the fundamental and harmonic frequencies. This causes the same power level not to be necessarily usable at both frequencies, thereby requiring adjustments to the input power.

There are still several improvements to be made to the measurement technique. First of all, it is important to be aware of the uncertainties of a particular measurement method, so that the potential error in the measurement result can be known. The technique should also be compared to other measurement techniques with respect to accuracy and suitability.

The technique itself could also be developed further. One obvious development would be the ability to measure the complex intermodulation response. This could provide further information to, e.g., make it possible to obtain the full impedance of

the antenna instead of only the magnitude of the reflection coefficient. The measurement setup could also be examined further to optimize the dynamic range.

As RFID is the most popular transponder application, further research of the technique relating to RFID would increase the usage of the technique drastically. So far, the technique has only been used in normalized radiation pattern measurements, so investigating the intermodulation properties of an RFID chip would enable the use of It could also be worth investigating if the technique would provide some relevant information that is not obtainable using the RFID reader itself to complement the information obtained from conventional RFID measurements.

However, further research should not be limited to transponder antennas. The technique could potentially be extended to other antennas. This would involve creating a nonlinear assembly that could be attached, e.g, using a SMA connector. The nonlinear assembly should have a characteristic impedance of 50 Ω over the operating bandwidth of the AUT and provide a strong intermodulation response. Designing such a device could be challenging, especially over a wide frequency band. Such a device would provide means to characterize electrically small antennas or other antennas where cable connection is problematic and further increase the usefulness of the intermodulation measurement technique.

Bibliography

[1] K. Finkenzeller, *RFID Handbook*, 3rd ed. John Wiley & Sons, Jun. 2010. [Online]. Available: http://dx.doi.org/10.1002/9780470665121

[2] J. Vogler, D. Maguire, and A. Steinhauer, "DINADE–a new interrogation, navigation and detection system," *Microwave Journal*, vol. 10, no. 4, pp. 2–6, Apr. 1967.

[3] J. Shefer and R. Klensch, "Harmonic radar helps autos avoid collisions," *IEEE Spectrum*, vol. 10, no. 5, pp. 38–45, May 1973.

[4] H. Staras and J. Shefer, "Harmonic radar detecting and ranging system for automotive vehicles," Patent, Dec., 1973, US Patent 3 781 879.

[5] RECCO Rescue System. Recco AB, Lidingö, Sweden. [Online]. Available: http://www.recco.com/about

[6] D. Mascanzoni and H. Wallin, "The harmonic radar: a new method of tracing insects in the field," *Ecological Entomology*, vol. 11, no. 4, pp. 387–390, Nov. 1986.

[7] J. Riley, P. Valeur, A. Smith, D. Reynolds, G. Poppy, and C. Löfstedt, "Harmonic radar as a means of tracking the pheromone-finding and pheromone-following flight of male moths," *Journal of Insect Behavior*, vol. 11, no. 2, pp. 287–296, 1998.

[8] Voyantic Ltd. Espoo, Finland. [Online]. Available: http://www.voyantic.com

[9] J. Appel-Hansen, "Accurate determination of gain and radiation patterns by radar cross-section measurements," *IEEE Transactions on Antennas and Propagation*, vol. 27, no. 5, pp. 640–646, Sep. 1979.

[10] M. Ritamäki, A. Ruhanen, V. Kukko, J. Miettinen, and L. H. Turner, "Contactless radiation pattern measurement method for UHF RFID transponders," *Electronics Letters*, vol. 41, no. 13, pp. 723–724, Jun. 2005.

[11] "IEEE standard definitions of terms for antennas," *IEEE Std 145-1993*, pp. 1–32, Apr. 2013.

[12] W. L. Stutzman and G. A. Thiele, *Antenna Theory and Design*, 3rd ed. Hoboken, NJ: John Wiley & Sons, 2012.

[13] H. Wheeler, "Fundamental limitations of small antennas," *Proceedings of the IRE*, vol. 35, no. 12, pp. 1479–1484, Dec. 1947.

[14] C. Icheln, J. Krogerus, and P. Vainikainen, "Use of balun chokes in small-antenna radiation measurements," *IEEE Transactions on Instrumentation and Measurement*, vol. 53, no. 2, pp. 498–506, Apr. 2004.

[15] P. Nikitin and K. Rao, "Gain measurement of antennas using RFID," in *IEEE International Symposium on Antennas and Propagation (APSURSI)*, Spokane, WA, Jul. 2011, pp. 1012–1015.

[16] D. D. King, "The measurement and interpretation of antenna scattering," *Proceedings of the IRE*, vol. 37, no. 7, pp. 770–777, Jul. 1949.

[17] R. F. Harrington, "Theory of loaded scatterers," *Proceedings of the Institution of Electrical Engineers*, vol. 111, no. 4, pp. 617–623, Apr. 1964.

[18] R. Garbacz, "Determination of antenna parameters by scattering cross-section measurements," *Proceedings of the Institution of Electrical Engineers*, vol. 111, no. 10, pp. 1679–1686, Oct. 1964.

[19] J. T. Mayhan, A. Dion, and A. Simmons, "A technique for measuring antenna drive port impedance using backscatter data," *IEEE Transactions on Antennas and Propagation*, vol. 42, no. 4, pp. 526–533, Apr. 1994.

[20] P. Pursula, D. Sandstrom, and K. Jaakkola, "Backscattering-based measurement of reactive antenna input impedance," *IEEE Transactions on Antennas and Propagation*, vol. 56, no. 2, pp. 469–474, Feb. 2008.

[21] D. M. Pozar, *Microwave Engineering*, 4th ed. Hoboken, NJ: John Wiley & Sons, 2011.

[22] D. E. N. Davies and H. Makridis, "Two-frequency secondary radar incorporating passive transponders," *Electronics Letters*, vol. 9, no. 25, pp. 592–593, Dec. 1973.

[23] J. Song, V. Viikari, N. Pesonen, I. Marttila, and H. Seppä, "Optimization of wireless sensors based on intermodulation communication," *IEEE Transactions on Microwave Theory and Techniques*, vol. 61, no. 9, pp. 3446–3452, Sep. 2013.

[24] V. Viikari, J. Song, and H. Seppä, "Passive wireless sensor platform utilizing a mechanical resonator," *IEEE Sensors Journal*, vol. 13, no. 4, pp. 1180–1186, Apr. 2013.

[25] V. Viikari, H. Seppä, and D.-W. Kim, "Intermodulation read-out principle for passive wireless sensors," *IEEE Transactions on Microwave Theory and Techniques*, vol. 59, no. 4, pp. 1025–1031, Apr. 2011.

[26] V. Viikari, H. Seppä, T. Mattila, and A. Alastalo, "Wireless ferroelectric resonating sensor," *IEEE Transactions on Ultrasonics, Ferroelectrics, and Frequency Control*, vol. 57, no. 4, pp. 785–791, Apr. 2010.

[27] V. Viikari and H. Seppä, "RFID MEMS sensor concept based on intermodulation distortion," *IEEE Sensors Journal*, vol. 9, no. 12, pp. 1918–1923, Dec. 2009.

[28] K. Rasilainen, J. Ilvonen, A. Lehtovuori, J.-M. Hannula, and V. Viikari, "On design and evaluation of harmonic transponders," *IEEE Transactions on Antennas and Propagation*, vol. 63, no. 1, pp. 15–23, Jan. 2015.

[29] K. Rasilainen, J. Ilvonen, and V. Viikari, "Antenna matching at harmonic operating frequencies to complex load impedance," *IEEE Antennas and Wireless Propagation Letters*, vol. 14, pp. 535–538, 2015.

[30] K. Rasilainen, J. Ilvonen, A. Lehtovuori, J.-M. Hannula, and V. Viikari, "Harmonic transponders: Performance and challenges," *Progress In Electromagnetics Research M*, vol. 41, pp. 139–147, 2015.

[31] J. Riley, A. Smith, D. Reynolds, A. Edwards, J. Osborne, I. Williams, N. Carreck, and G. Poppy, "Tracking bees with harmonic radar," *Nature*, vol. 379, no. 6560, pp. 29–30, Jan. 1996.

[32] E. A. Capaldi, A. D. Smith, J. L. Osborne, S. E. Fahrbach, S. M. Farris, D. R. Reynolds, A. S. Edwards, A. Martin, G. E. Robinson, G. M. Poppy, and J. R. Riley, "Ontogeny of orientation flight in the honeybee revealed by harmonic radar," *Nature*, vol. 403, no. 6769, pp. 537–540, Feb. 2000.

[33] E. T. Cant, A. D. Smith, D. R. Reynolds, and J. L. Osborne, "Tracking butterfly flight paths across the landscape with harmonic radar," *Proceedings. Biological sciences / The Royal Society*, vol. 272, no. 1565, pp. 785–790, Apr. 2005.

[34] R. Brazee, E. Miller, M. Reding, M. Klein, B. Nudd, and H. Zhu, "A transponder for harmonic radar tracking of the black vine weevil in behavioral research," *Transactions of the ASAE*, vol. 48, no. 2, pp. 831–838, Mar. 2005.

[35] H. Aumann, E. Kus, B. Cline, and N. W. Emanetoglu, "A low-cost harmonic radar for tracking very small tagged amphibians," in *IEEE International Instrumentation and Measurement Technology Conference (I2MTC)*, no. 3, Minneapolis, MN, USA, May 2013, pp. 234–237.

[36] J. R. Riley and A. D. Smith, "Design considerations for an harmonic radar to investigate the flight of insects at low altitude," *Computers and Electronics in Agriculture*, vol. 35, no. 2-3, pp. 151–169, Aug. 2002.

[37] J.-M. Hannula, K. Rasilainen, and V. Viikari, "Characterization of transponder antennas using intermodulation response," *IEEE Transactions on Antennas and Propagation*, 2015. [Online]. Available: http://dx.doi.org/10.1109/TAP.2015.2414438

[38] *SMV2019 to SMV2023 Series: Hyperabrupt Junction Tuning Varactors*, Skyworks Solutions, Inc., Oct. 2014. [Online]. Available: http://www.skyworksinc.com/Product/668/SMV2019_Series

[39] LabVIEW System Design Software. National Instruments. Austin, Texas, USA. [Online]. Available: http://www.ni.com/labview/

[40] MATLAB. MathWorks Inc. Natick, Massachusetts, USA. [Online]. Available: http://se.mathworks.com/products/matlab/

[41] SEMCAD X, ver. 14.8. Aletsch, Schmid & Partner Engineering AG. Zurich, Switzerland. [Online]. Available: http://www.semcad.com